Report CE/ST 36

report submitted to American Institute of Steel Construction

Effects of Slab Post-tensioning on Supporting Steel Beams

Bhavna Sharma, M.Sc.
Kent A. Harries, Ph.D., FACI, P.Eng.

March 2007

school of engineering
civil and environmental engineering
structural engineering and mechanics
Watkins-Haggart Structural Engineering Laboratory

Effects of Slab Post-tensioning on Supporting Steel Beams

Bhavna Sharma and Kent A. Harries, Ph.D., FACI, P.Eng.
University of Pittsburgh
Department of Civil and Environmental Engineering
Pittsburgh PA 15261

Acknowledgements
This study was carried out with support from the American Institute of Steel Construction (AISC). In this regard, the authors wish to acknowledge Tom Schalfly, Bill Pascoli, John Cross and Charles Carter. Charles Churches Sr. of Churches Engineering, Washington PA, is the EOR for the project. His support and the information he provided is gratefully acknowledged. Eric Campbell of Ionadi Construction, Pittsburgh PA, was the site supervisor; his assistance was invaluable to the study. The building is owned by Real Estate Enterprises, Pittsburgh PA; Kai Olander is acknowledged for providing access to the site and test structure. University of Pittsburgh graduate and undergraduate students Keith Coogler, Patrick Minnaugh, Derek Mitch, Mark Beacraft, Louis Gualtieri and Lisa Abraham assisted in various aspects of instrumentation and data acquisition. The findings of this report do not necessarily reflect the opinions of those acknowledged above.

This research was sponsored by the American Institute of Steel Construction. The opinions, findings and conclusions expressed in this report are those of the authors and not necessarily those of AISC or The University of Pittsburgh. This report does not comprise a standard, specification or regulation.

this page intentionally left blank

Table of Contents

List of Figures

List of Tables

1. Preamble

AISC Design Guide 18, *Steel Framed Open-Deck Parking Deck Structures* (Churches et al. 2003), discusses the use of cast-in-place post tensioned slabs in steel framed parking structures. In Section 3.3.2.1, the authors reflect on the manner in which the post-tensioning force is carried by the supporting beam: in a non composite or composite manner. They conclude that the post-tensioning force is carried almost entirely in a composite manner (minus effects of shrinkage and elastic shortening). This conclusion is based on results of unpublished research (as reported) and is corroborated by earlier design guidance provided by Bakota (1988).

1.1 Objective

The objective of this field study is to quantitatively assess the effect that slab post-tensioning forces have on their supporting steel members.

2. Current Practice and Literature Review

Cast-in-place post-tensioned concrete slabs on steel girders are an attractive alternative for parking structures. The use of post-tensioned slabs permits somewhat longer spans to be achieved but primarily enhances the durability of the slab system, affecting superior crack control. Investigation of the effects of the post-tensioning stress on the composite behavior of the beams has been explored but not published. Current practice, as promulgated in AISC Design Guide 18, *Steel Framed Open-Deck Parking Deck Structures* (Churches et al. 2003) assumes that the composite beams experience a small amount of compressive stress from the post-tensioning of the slab along the length of the beam. Design Guide 18 notes that unpublished testing by Mulach Steel Corporation demonstrated a stress increase of 3% in the composite beams under dead load conditions.

Bakota (1988) explores the design of a post-tensioned parking deck and analyzes the effects of post-tension stresses on the composite beam. The author notes various design criteria for a post-tensioned deck and that an effective post-tension stress of 100 psi in the transverse shrinkage and temperature direction reduces the effects of the post tensioning parallel to the beam. Bakota presents equations to determine the long-term stresses and deflections. He concludes that the post-tension forces in the deck create long-term beam and slab stresses due to differential volume changes.

Steel framed parking structures, in general, where introduced in the literature in the 1960's (Sontag 1970; "New" 1974). Frequent references and case studies appear in the literature through today: in North America, typically appearing in *Modern Steel Construction*; in Europe, in *Acier-Stahl-Steel*; and elsewhere including a number of references in the South African Journal *Steel Construction*. In addition to Design Guide 18, AISC promulgates *Innovative Solution in Steel: Open Deck Parking Structures* (Troup and Cross 2003). Available references in the literature primarily address precast concrete decks on steel frames (e.g.: Simon 2001; Englot and Davidson 2001). A review of available literature revealed no additional publications relating specifically to cast-in-place post-tensioned concrete decks on steel frames.

3. Test Structure – 450 Melwood Avenue, Pittsburgh PA

The test structure reported in this study is a single story steel parking structure having a post-tensioned composite concrete deck. The structure is located behind 450 Melwood Avenue in the North Oakland area of Pittsburgh (Figure 3.1). The structure, shown complete in Figure 3.2, is a single story steel frame over a slab on-grade. Parking is provided on both levels although there is no connecting ramp. Separate entrances are provided for the grade and deck parking.

Figure 3.1 450 Melwood Avenue, Pittsburgh PA.

Overall view of 11 bay parking structure looking West from across railway right-of-way.

Interior of parking structure.

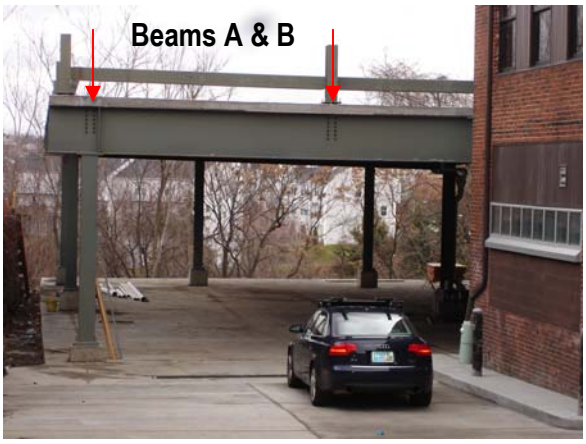

Exterior of parking structure at Beams A and B.

Figure 3.2 Completed parking structure at 450 Melwood Ave.

As shown in Figure 3.3, the structure has eleven bays (ten measuring 20'-0" and the first measuring 15' 0") in the N-S direction and two bays in the E-W direction: bay 1-2 measuring 45'-2" and bay 2-3 measuring 35'-2". There is a 10' cantilever beyond column line 3. All columns are W12x65 and the beams spanning bay 1-2 are W24x76 at Beams C and D and W24x68 at Beam B. Where beams frame into girders, a simple shear connection is provided (Figure 3.4, lower left). Beams that frame into columns (all strong axis, in this case) are provided with angles at both flanges resulting in a partially-restrained connection (Figure 3.4, lower right). The beams considered in this study span bay 1-2 at column lines B, C and D. These beams will be referred to as Beams B, C and D, respectively as indicated in Figure 3.3.

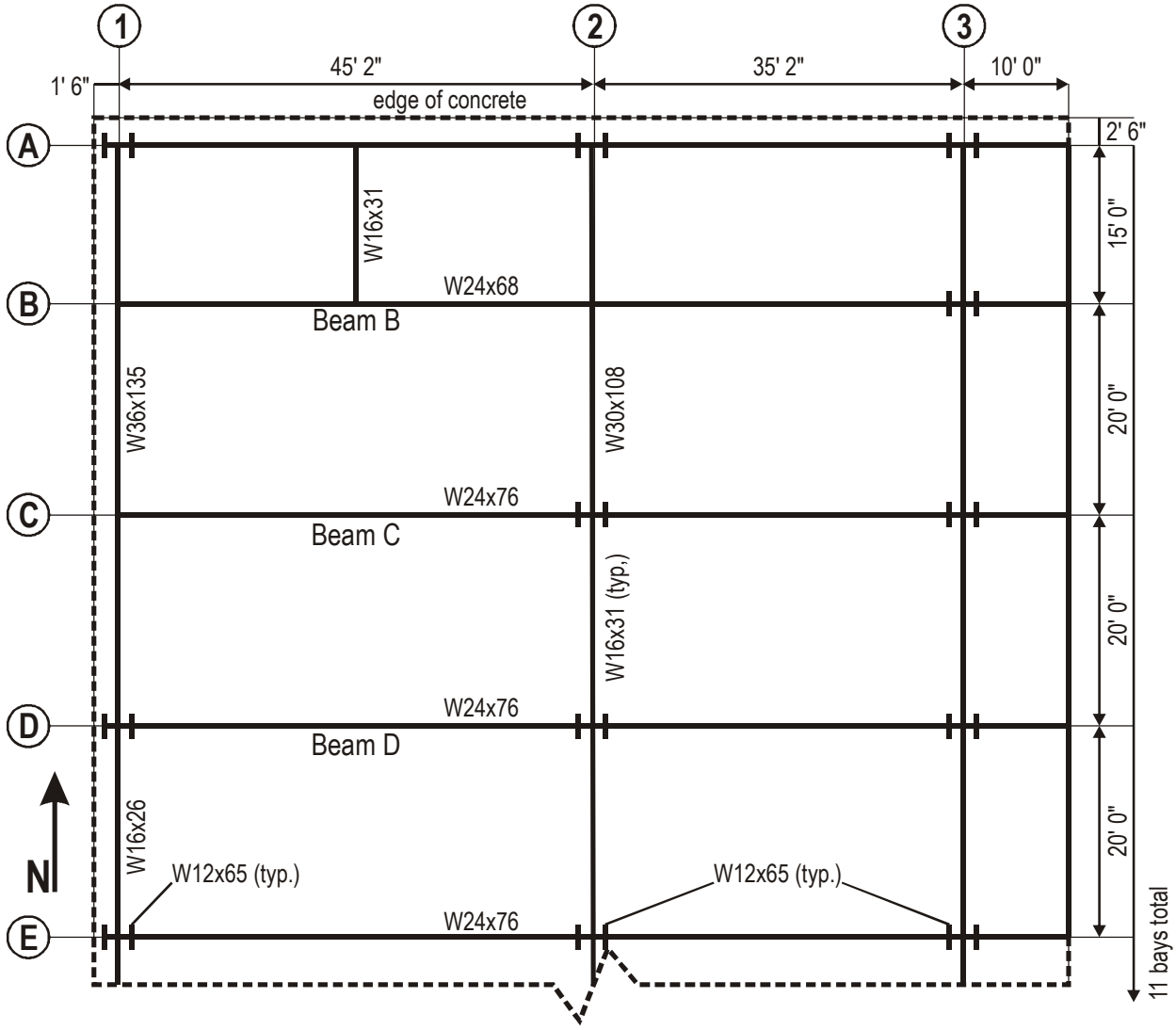

Figure 3.3 Structural steel framing plan.

The cast-in-place concrete deck is a 6" post-tensioned concrete slab. Reinforcing details of the deck are shown in Figure 3.5 and views of the deck prior to concrete placement is shown in Figure 3.6. Single, double and triple strands are arranged as shown in Figure 3.5. The concrete stress due to initial post tensioning is 330 psi in the N-S direction and 168 psi in the E-W direction. Mild steel is arranged primarily for crack control as indicated in Figure 3.5. Additionally, as shown in Figure 3.6, 5/8" x 3" shear studs are provided along all beams in bay 1-2 at a spacing of 10".

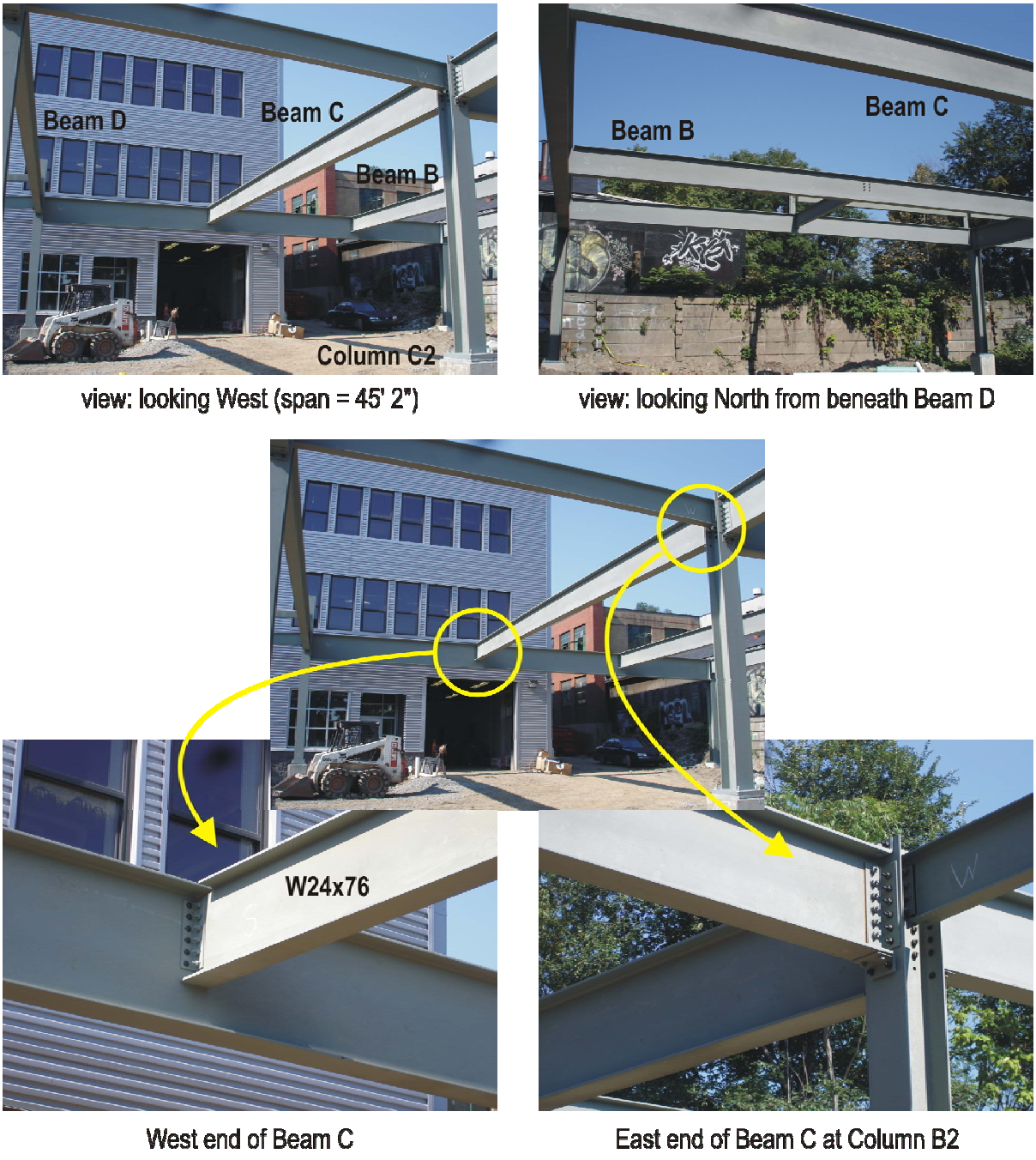

Figure 3.4 Steel superstructure.

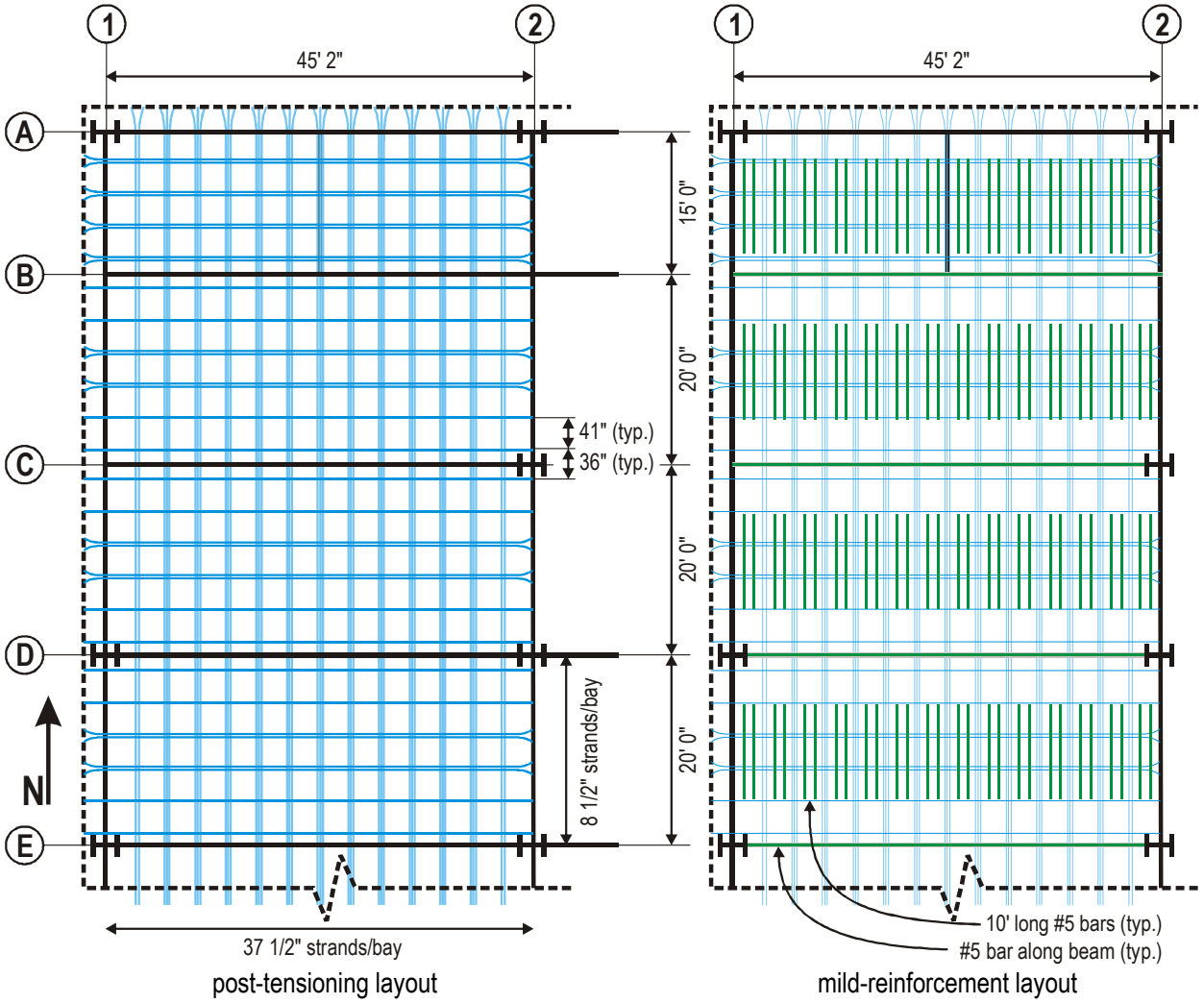

Figure 3.5 PT tendon and reinforcing steel plan.

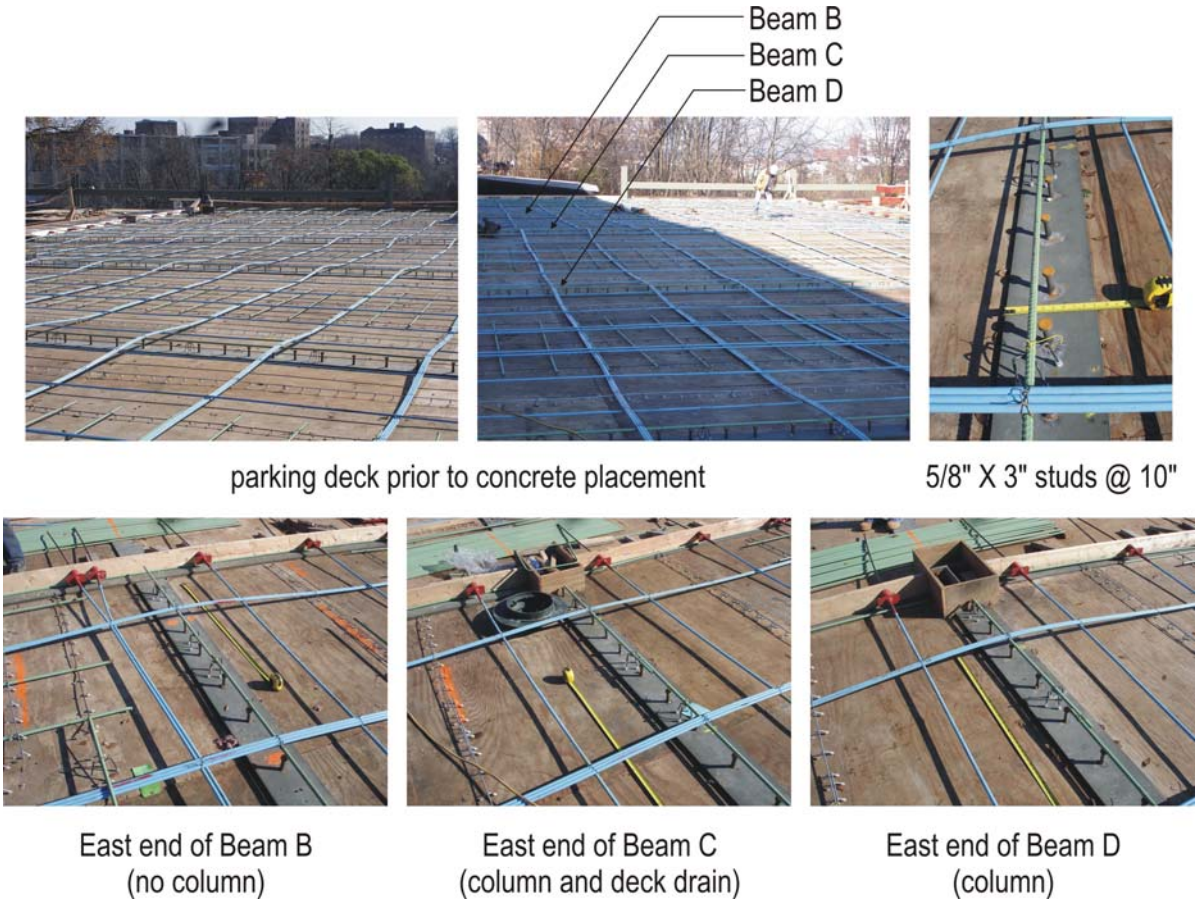

Figure 3.6 Reinforcing bar and strand layout prior to concrete placement (November 21, 2006).

3.1 Structural Steel

All structural steel considered in this study are ASTM A992 Grade 50 members. No material tests were conducted on this steel.

3.2 Concrete

The concrete in bay 1-2 was placed beginning at 7 am on November 22, 2006. The concreting in the vicinity of the test beams was completed by 8:30 am. The specified concrete compressive strength was 5000 psi. Both the University of Pittsburgh team and the contractor placed test cylinders. Table 3.1 provides concrete material strength reported by both laboratories.

Table 3.1 Concrete test results

Test reported by…	age of concrete	concrete compressive strength
contractor lab	5 days	3450 psi (std dev = 570 psi)[1]
University of Pittsburgh	5 days	2010 psi (std dev = 752 psi)
University of Pittsburgh	28 days	5070 psi (std dev = 11 psi)

[1] approximate values, not verified by authors

Following placement on November 22, 2006, the ambient temperature reported for Pittsburgh is given in Figure 5.1 (top). As a rule-of-thumb, the temperature needs to exceed 45°F otherwise curing is retarded. Curing is arrested when the temperature falls below 32°F. The cylinders tested by the University of Pittsburgh were left on site in ambient conditions until the morning of November 27. The contractor cylinders, on the other hand were removed

from the site November 24. It is believed that these latter cylinders were maintained in a more controlled environment until tested on November 27. This series of events explains the discrepancy in concrete material strengths obtained at 5 day testing. As no curing mats were used, it is proposed that the University of Pittsburgh results are more representative of the *in situ* concrete properties.

3.3 Post Tensioning Strand

All post tensioning strand used in the deck was ½" 270 ksi seven wire prestressing strand (A_{ps} = 0.153 in^2). The strand was enclosed in a greased plastic sheath. No material tests were conducted on this steel. The post-tensioning operation is described in Section 6.1.

3.4 Mild Reinforcement

All mild reinforcement in the deck is #5 epoxy coated reinforcing bar having a nominal yield strength of f_y = 60 ksi. No material tests were conducted on this steel. The mild steel was provided only for crack control and is not sufficient to affect the deck structural behavior.

4. Instrumentation

Electrical resistance strain gages were used to determine strain in Beams B, C and D. As shown in Figure 4.1, gages were located at five sections along beams B and D and at three sections along Beam C[1]. At each section, three gages were provided as shown in Figure 4.2: one on the bottom of the top flange, one on the top of the bottom flange and one at the midheight of the web. Gages are designated by their beam designation and the number 1 through 15 as shown in Figure 4.1 (for example, gage D8 is the web midheight gage at midspan of Beam D) All gages were oriented longitudinally to capture flexure-induced strains. The flange gages were located 1.5" from the face of the web so as to avoid both the K-region fillet and the lapping of the deck form (Figure 4.2).

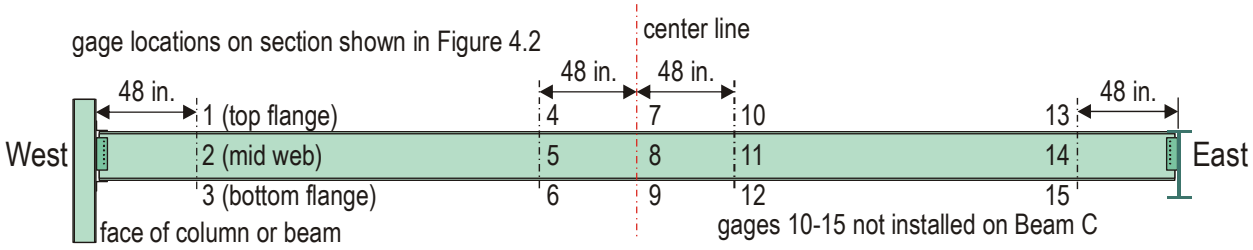

Figure 4.1 Strain gage layout.

[1] failure of the strain gage welder did not allow the final two sections (gages 10-15) on Beam C to be instrumented.

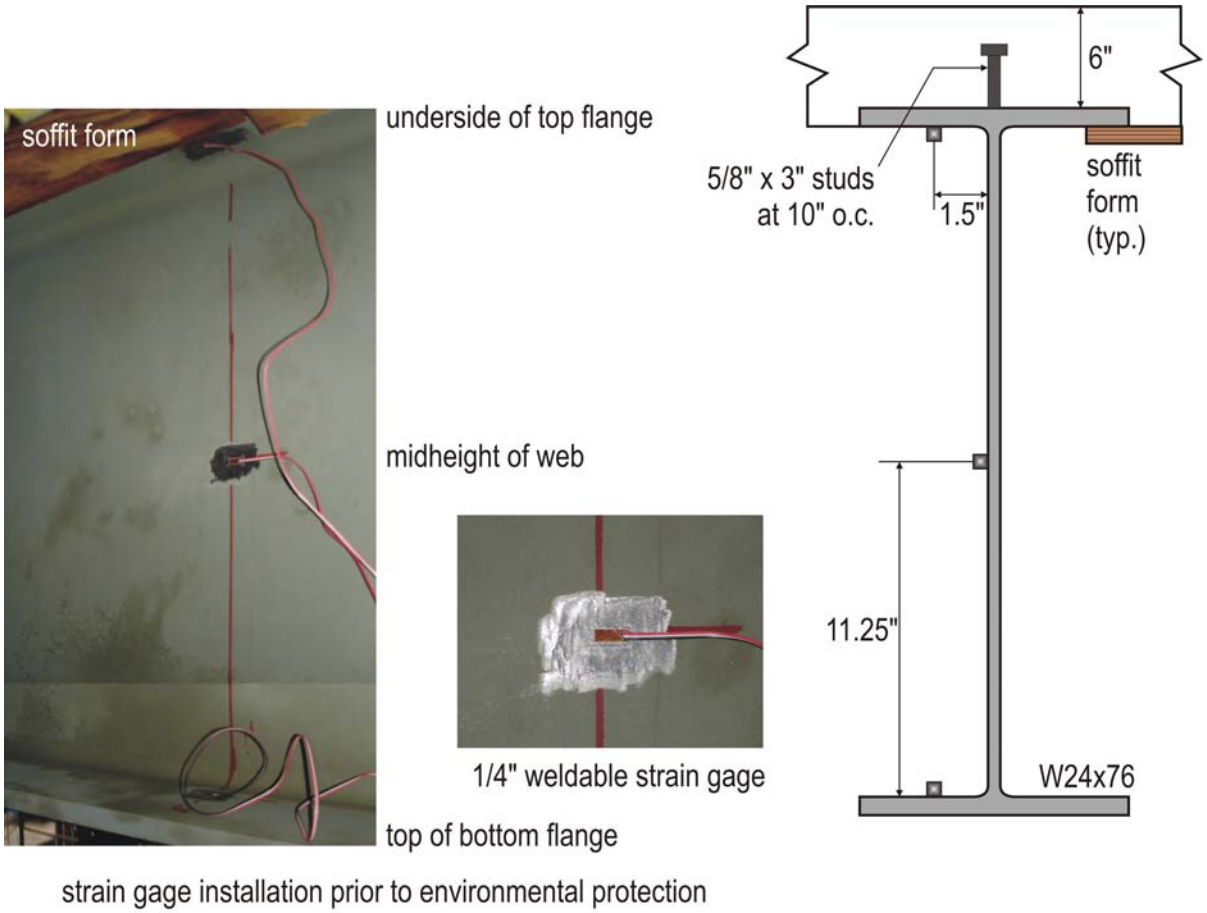

Figure 4.2 Strain gage installation (Beam B midspan shown)

.

All gages used were MicroMeasurements CEA-06-W25A-120 gages. These are ¼" long 120Ω electrical resistance strain gages mounted on an "Iconel" metal carrier which is subsequently spot-welded to the substrate steel. The gages are applied to smooth bright steel as shown in figure 4.2. The gages are self-temperature compensating and matched to a structural steel substrate. All gages were wired with factory-installed 24" long 26-gage lead wires. The gage wires were subsequently connected to screw terminals and 60" lead wires were used to connect the terminals to the data acquisition instrument. Thus all gages had an identical installation utilizing less than 10' of lead wire.

Once installed, gages were protected with MicroMeasurements M-Coat D, a dense air-drying acrylic, and M-Coat F, a butyl-rubber sealant. In this manner the gages are both protected from moisture and physical abrasion. All gages and wiring were subsequently protected with an asphaltic flashing tape. The complete installation with the screw terminals is seen in the left-hand image in Figure 4.3.

It was not possible to control all field conditions at all times. Following gage installation, the formwork contractor installed flange shores. In many cases, the shores were located very near gage locations. In two cases, shown in Figure 4.3, these shores were placed directly on top of the gages! Section 6.3 addresses the integrity of the strain gages through the test program.

Figure 4.3 Installations of formwork shores near and directly on top of strain gages.

All gage data was collected on the same Vishay P3 (S/N 164882) 4-channel strain gage indicator (Figure 4.4). Channels 1 through 3 were connected to the three gages at each beam section and data was manually recorded. In all cases, gages were always recorded by the same channel having balancing and offset functions disabled. In this manner gage readings through time are made consistent and comparable.

Figure 4.4 Vishay P3 4-channel strain gage indicator (images: Vishay).

The readings taken November 21, 2006 (Milestone A) were selected to be the "zero" readings. The load on the beams at this time was only the beam self weight. In addition to calibrating by this zero reading, the ambient temperature at milestone A, 38°F, was taken as the baseline temperature. All subsequent data was corrected using a coefficient of thermal expansion for steel (matched by the gages) of 6 x 10^{-6}/°F. The temperature history for Pittsburgh during the test program is shown in Figure 5.1.

5. Test Program

Table 5.1 provides a summary of the test program milestones in addition to the age of the deck and ambient temperature for all data acquisition tasks. Tests are defined as A through J as indicated in Table 5.1. The ambient (unseasonably warm) temperature history for Pittsburgh over the duration of the test program, November 20, 2006 through January 12, 2007, is provided in Figure 5.1. Photographs of selected milestones are shown in Figures 5.2 through 5.5, these include: placing the concrete (Figure 5.2); pulling the post-tensioning strand (Figure 5.3); the support condition of beam B at Milestone F (Figure 5.4); and, Dr. Harries taking readings at Milestone H (Figure 5.5).

Table 5.1 Test Program Milestones.

Milestone		Date	Concrete Age	Ambient Temperature
	steel erected	September 26		
	formwork erected	November 9		
	strain gages installed	November 10 - 14		
	data acquisition: initial zero reading	November 15		begin: 40 °F end: 46 °F
	data acquisition: second zero reading	November 17		43°F
	form shore installed	November 20		
A	data acquisition: third zero reading	November 21		38°F
	concrete placed	November 22 (7 am)	0	begin: 33°F max: 52°F end: 46°F
B	data acquisition: concrete placed	November 22 (2 pm)	≈ 7 hours	48°F
	PT strands stressed	November 27	5 days	
C*	data acquisition: during PT stressing operation	November 27	5 days	48°F
C	data acquisition: following initial PT force application	November 27	5 days	62°F
D	data acquisition: fully shored	November 30	8 days	67°F
E	data acquisition: fully shored	December 8	16 days	29°F
	remove shores under Beams C and D	December 14	22 days	
F	data acquisition: Beam B partially shored; C and D unshored	December 15	23 days	55°F
	all shores removed	December 19	27 days	
	28-day concrete cylinder tests	December 20	28 days	
G	data acquisition: full dead load	December 21	29 days	46°F
H	data acquisition: full dead load	December 23	31 days	46°F
I	data acquisition: full dead load only	December 30	38 days	52°F
I*	data acquisition: AUDI A4 live load only	December 30	38 days	52°F
J	data acquisition: full dead load only	January 12	51 days	49°F
J*	data acquisition: two vehicle live load only	January 12	51 days	49°F

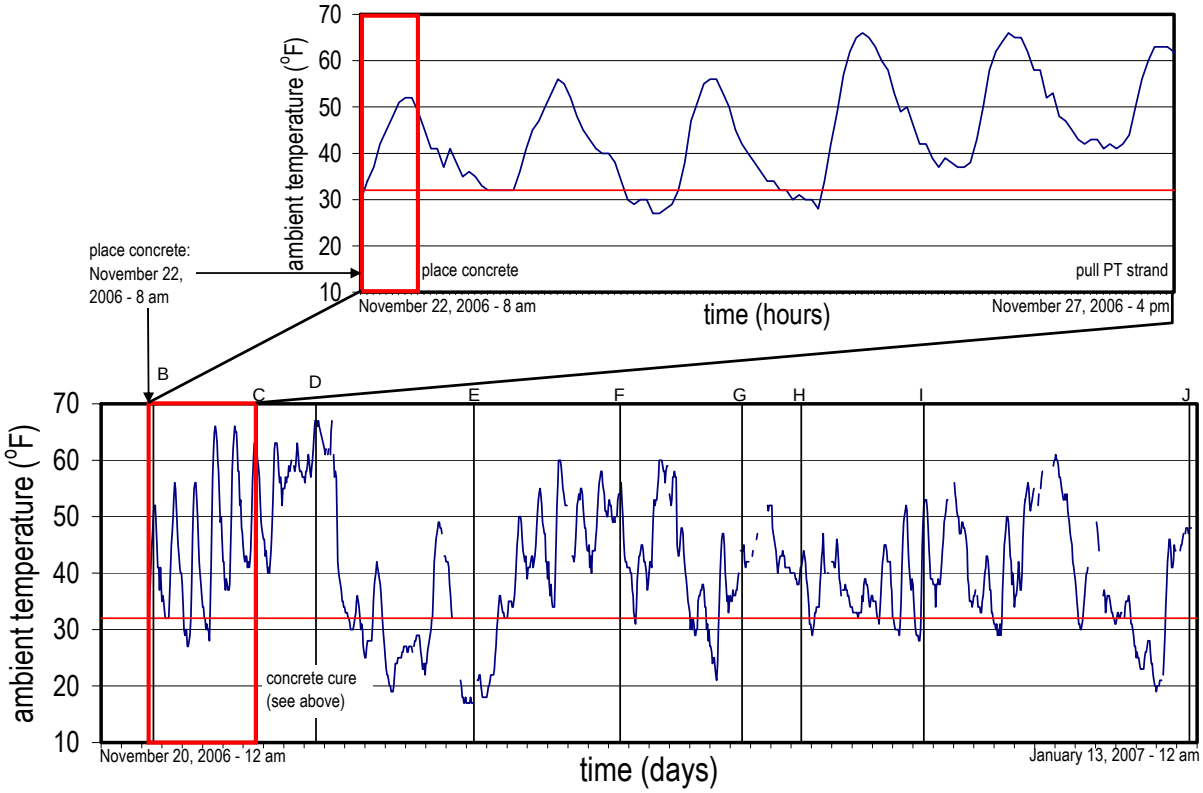

Figure 5.1 Pittsburgh ambient hourly temperatures (NOAA).

Figure 5.2 Placing concrete: November 22, 2006.

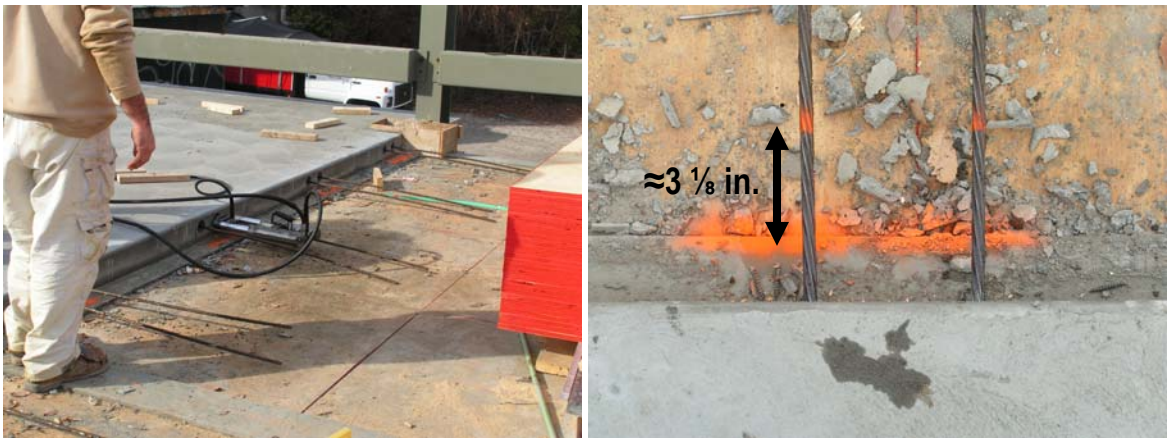

5.3 Pulling the PT strand: November 27, 2006.

Figure 5.4 Shoring condition at Beam B: December 14 through 19, 2006.

Figure 5.5 Taking readings: December 23, 2006.

6. Test Results

The fundamental data collected in this work are the longitudinal strains observed at each of the 39 strain gages. These strains are reported as sectional strain diagrams in Figure 6.1. Figure 6.1 reports Milestones B, C, F, H, I and J as being representative of the stages of the structure's construction and initial operation. All data is provided *relative to Milestone A* and thus the strains reported do not include the strains associated with the dead load of the beam itself (including some minor construction loads associated with the formwork). Based on a simple span, the maximum stress and strain (i.e.: that at midspan) associated with the beam dead load, at the location of the gages (inside face of flanges) are 1195 psi and 41 microstrain, respectively. Based on a fixed-fixed span, these values fall to 398 psi and 14 microstrain, respectively. These values have not been added to the data shown in Figure 6.1 since the exact support conditions are uncertain. Additionally, all data in Figure 6.1 has been corrected for ambient temperature as described in Section 4 and erroneous data has been purged as described in Section 6.3. Finally, the strain profiles shown in Figure 6.1 are drawn to scale; the observed strain at the top of the lower flange is shown. The reader is reminded that the top and bottom gage locations are on the inside of the flange and therefore do not represent the absolute maximum value of strain observed in the steel section. Tabulated strain observations for all milestones are provided in Appendix A.

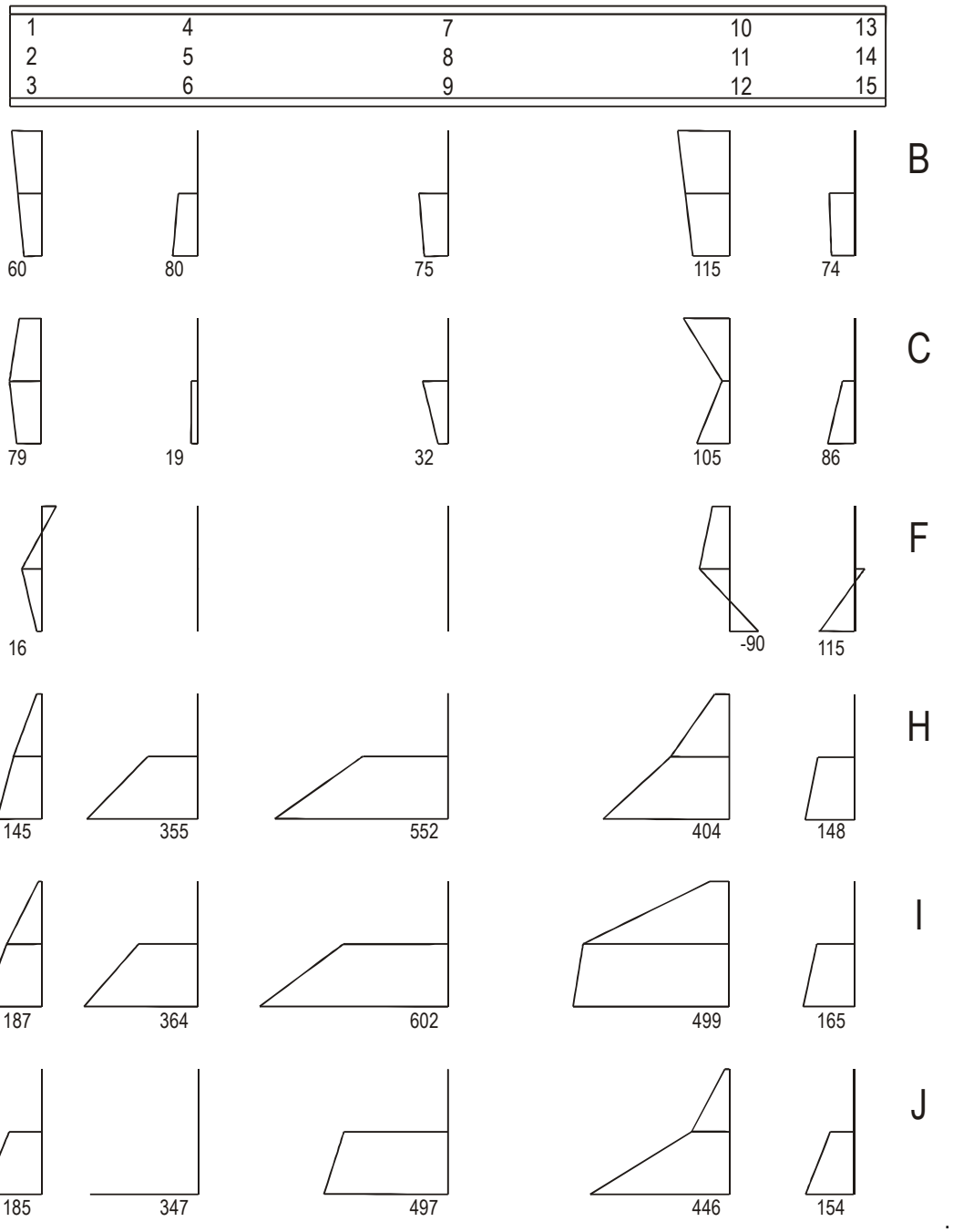

Figure 6.1(a) Strain profiles for Beam B.

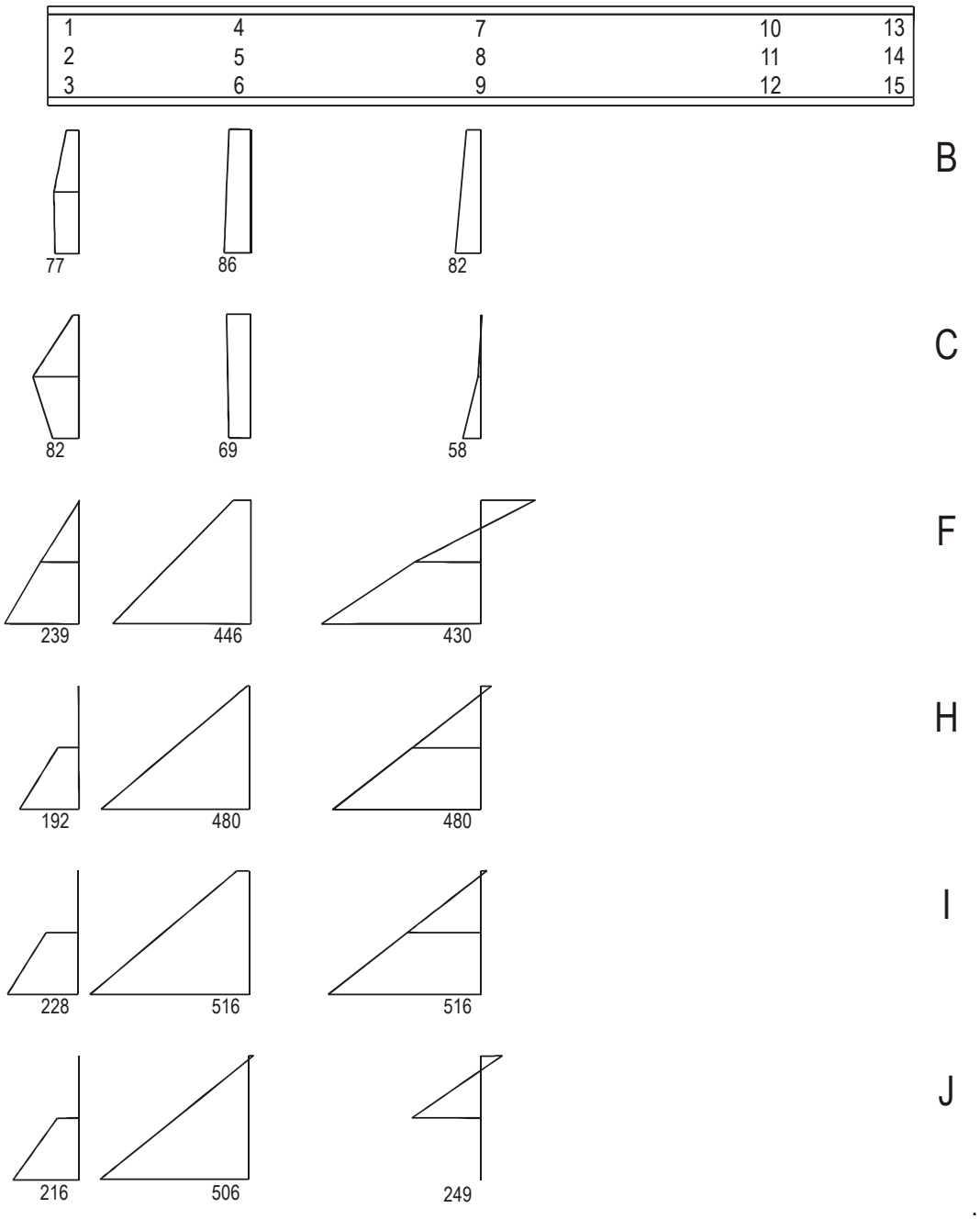

Figure 6.1(b) Strain profiles for Beam C.

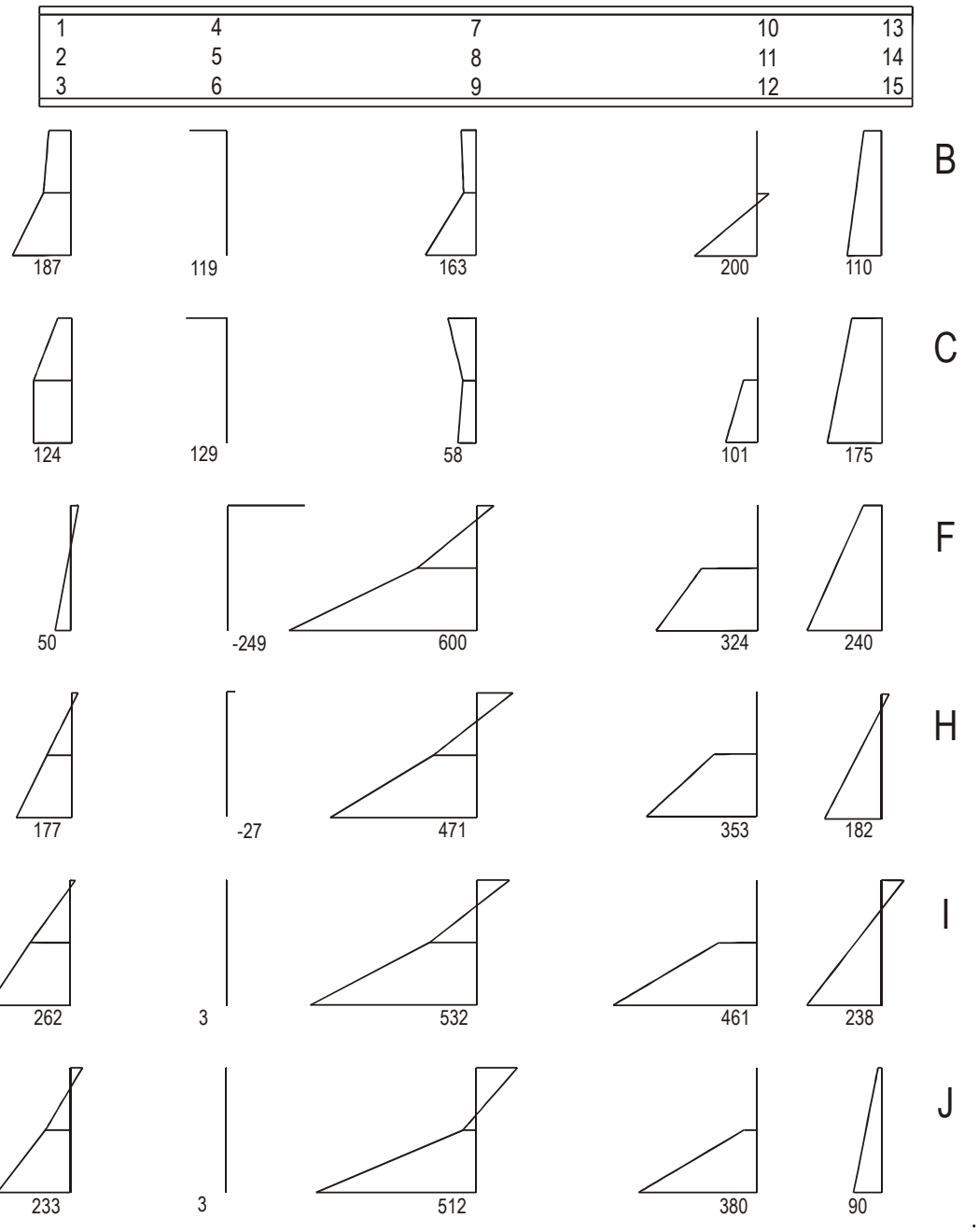

Figure 6.1(c) Strain profiles for Beam D.

6.1 Post-Tensioning Operation – November 27, 2006.

Post-tensioning bay 1-2 was conducted in the afternoon of November 27, 2006. The concrete was 5 days old. Concrete strength data is provided in Table 3.1. Tensioning began at beam line A and progressed southward along the deck (see Figure 5.3, showing the post-tensioning operation near beam A). The ½" unbonded strands were pulled from their end along girder line 2 with their anchorage at girder line 1. Each strand was pulled to a stress of 216 ksi ($0.80f_{pu}$) resulting in an initial strand force of 33000 lbs. Friction and seating losses result in an initial prestress in the tendons following lock-off of approximately 198 ksi ($0.73f_{pu}$ = 30200 lbs; see calculation shown below). Long-term losses associated with concrete creep and shrinkage (also shown below) amount to an additional loss of approximately 9 ksi ($0.03f_{pu}$) resulting in a final long-term effective prestress of approximately 189 ksi ($0.70f_{pu}$) in the E-W direction. The resulting compressive stress in the concrete in the E-W direction is 160 psi.

Calculations – Losses in unbonded post tensioned strand

Friction Losses (ACI 318-05 18.6.2)

$$P_{px} = P_{pj} e^{-(K\ell_{px} + \mu_p \alpha_{px})} = (216 \text{ ksi})\, e^{-[(0.001)45 + (0.1)0]} = 206 \text{ ksi}$$ …friction loss, **FR = 10.0 ksi** = $0.037f_{pu}$

where P_{px} is the effective PT force at distance ℓ_{px} from the jacking end;
P_{pj} is the jacking force; in this case $P_{pj} = 0.80f_{pu}$ = 216 ksi;
K is the wobble coefficient given by ACI 318 Table R18.6.2, taken as 0.001 in this case; and,
$\mu_p\alpha_{px}$ reflects losses associated with the curvature of the tendon; in this case $\alpha_{px} = 0$.

Thus the effective PT force at the anchorage is 206 ksi and the average PT force over the tendon length is 212 ksi when the anchorage is locked off.

Seating Losses

It is typically assumed that lock-off results in an anchorage set of approximately ¼". Using a value of ℓ_{px} = 45', this results in a loss of: [0.25/(45 x 12)] x 29,000 = 13.4 ksi

…seating loss, **LO = 13.4 ksi** = $0.050f_{pu}$

Shrinkage Losses (Aalami 2004)

$SH = 8.2 \times 10^{-6} K_{SH} E_s (1 - 0.06(V/S))(100\text{-}RH) = 8.2 \times 10^{-6} (1.0)(29{,}000)(1 - 0.06(0.5/2))(100\text{-}70) = 7.0$ ksi

…shrinkage loss, **SH = 7.0 ksi** = $0.026f_{pu}$

where V/S is the volume to surface area ratio of the concrete element;
RH is the ambient relative humidity, taken as 70% for Pittsburgh; and,
K_{SH} is the shrinkage coefficient appropriately taken as unity in a case with no accelerated curing.

Creep Losses (Aalami 2004)

$CR = K_{cr}(E_s/E_c)f_{cpa} = 2(7.2)[8 \times 0.153 \times (218 - 18.4)/(240 \times 6)] = 2.4$ ksi

…creep loss, **CR = 2.4 ksi** = $0.009f_{pu}$

where f_{cpa} is the effective prestress in the slab prior to long-term losses; and,
K_{cr} is the creep coefficient appropriately taken as 2 in this case.

Following post-tensioning in the E-W direction, the N-S strands were pulled. The resulting concrete stress in the N-S direction following lock-off is approximately 330 psi (based on a stress in the tendon of $0.70f_{pu}$). In reality, this value is likely considerably lower due to the length of tendons (approximately 220') and the wobble introduced by the changing slope of the deck in the N-S direction. Control of the stressing operation was through a pressure limiting pump operating the stressing jack. Strand elongation – expected to be 3.125" – was also verified at each strand (see Figure 5.3). In the 450 Melwood structure, no moist or accelerated curing techniques were used which resulted in greater shrinkage losses than are typically expected

Continuous monitoring of gages 4-6 on Beam B and 7-9 on Beam D was carried out throughout the post-tensioning operation. Gage readings were recorded at a rate of 1Hz from throughout the operation. Strain-time histories for all six gages are shown in Figure 6.2. Figure 6-2 shows *relative* strains through the post-tensioning operation. All gage data was zeroed at 12:50 pm – just prior to the initiation of the post-tensioning operation at Beam A.

The post-tensioning of the strands immediately above Beams B and D occurred at approximately 12:59 pm and 1:18 pm, respectively. In each case approximately one half of the eventual strain had been developed at these times. It is additionally clear from Figure 6.2 that only the strands tributary to a girder affect the strain in that girder. It is noted that the "initial condition" of Beam D strains in the lower graph in Figure 6.2 is essentially the same as those of Beam B. Little effect from the stressing of Beam B (or Beam C, between these girders) is apparent on the behavior of Beam D. Additionally, despite the observations of Bakota (1988) reported in Section 2, little effect on the observed beam strains were observed following pulling of the perpendicular (N-S) post-tensioning.

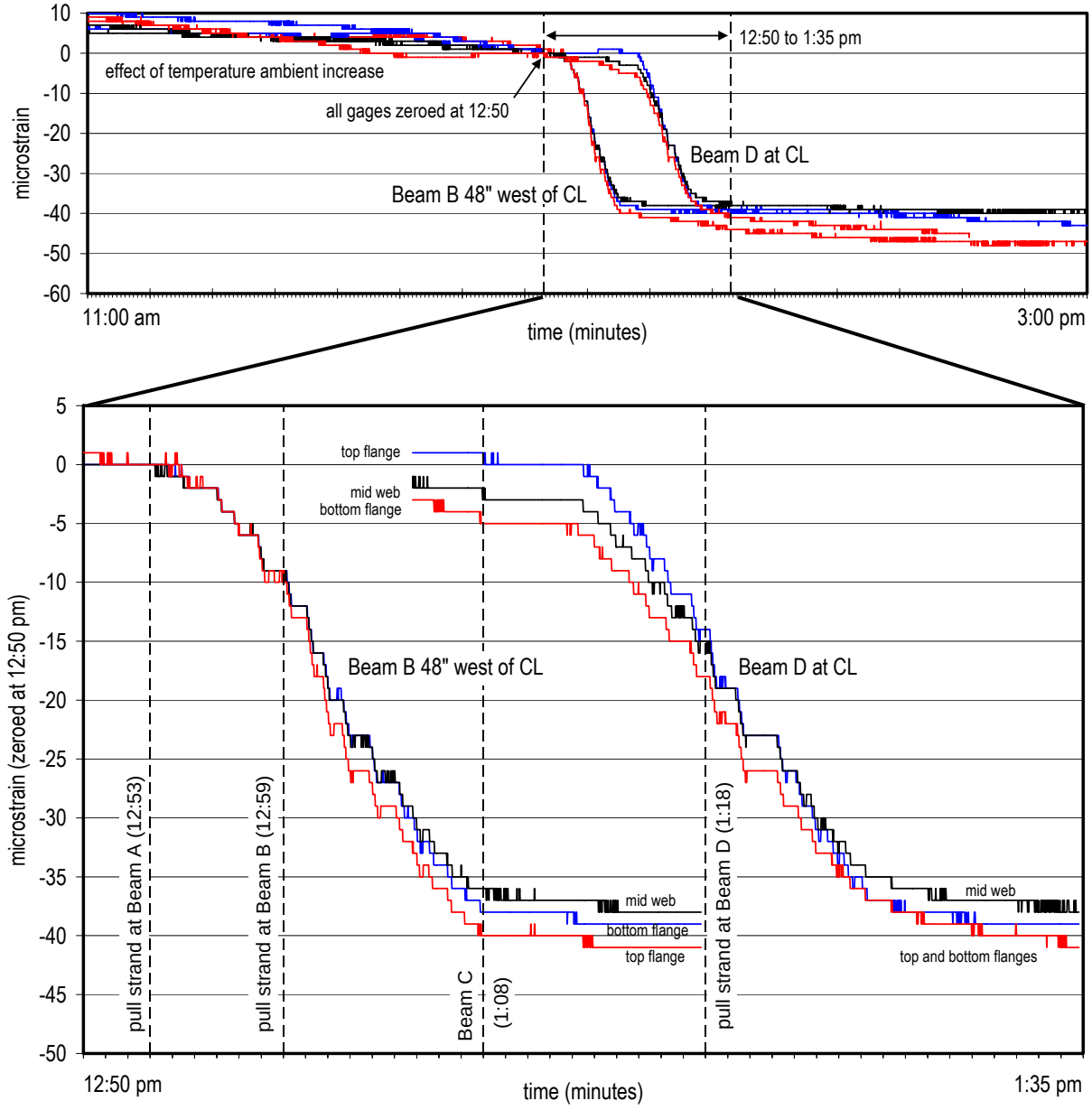

Figure 6.2 Observed strains during post-tensioning operation.

6.2 Live Load Tests

6.2.1. "Audi" Test – December 30, 2006

An initial live load test to simply assess the composite behavior of the deck (and to determine the needs for a more substantial live load test) was conducted on Beam D December 30, 2006. In this test, An AUDI A4 having specified front and rear GAVW of 1960 lbs and 1942 lbs, respectively, was positioned over the center of Beam D as shown in Figure 6.3. The strains resulting only from the application of the live load in the constant moment region (gages 7-9) are shown. From the live load strain distribution obtained, the location of the beam neutral axis was determined and the resulting applied moment found as indicated in the calculations shown below. Based on ACI-prescribed design assumptions (effective slab width, b_{eff} = 105"), the maximum live load moment is 195,800 lb-in – this may be interpreted as a lower-bound value. Based on AISC-prescribed design assumptions, the entire tributary slab width is

effective (b_{eff} = 240") and the maximum live load moment is 212,250 lb-in – this may be interpreted as an upper-bound value. The appropriate value for the effective slab width is discussed in Section 7.1.

As shown in Figure 6.3, the live load moment resulting from the four-point bending case applied is 458,484 lb-in for a simple span and 203,290 lb-in for a span having fixed supports. Based on the observed strain behavior, Beam D is clearly behaving as a composite member having ends largely restrained from rotation. This result is considered reasonable based on the relatively low stress level applied and the presence of clip angles on both flanges at both ends of Beam D.

Calculations – Apparent live load moment

location of neutral axis (NA) determined:	y = 22.36"
distance from NA to top of bottom flange:	y = 22.36 - 0.68 = 21.68"
observed stress at top of bottom flange (gage 9):	f_s = 25 microstrain x 29,000 ksi = 725 psi
section moment:	$M = f_s(I/y)$
modular ratio:	$n = E_s/E_c$ = 7.2 ...assumed
Case 1 – ACI prescribed effective slab width	
effective width of slab:	b_{eff} = 105"
resulting transformed moment of inertia:	I = 5855 in^4
section moment:	$M = f_s(I/y)$ = (725)(5855/21.68) = 195 800 lb-in
Case 2 – effective slab width equal to girder spacing	
effective width of slab:	b_{eff} = S = 240"
resulting transformed moment of inertia:	I = 6347 in^4
section moment:	$M = f_s(I/y)$ = (725)(6347 /21.68) = 212 250 lb-in

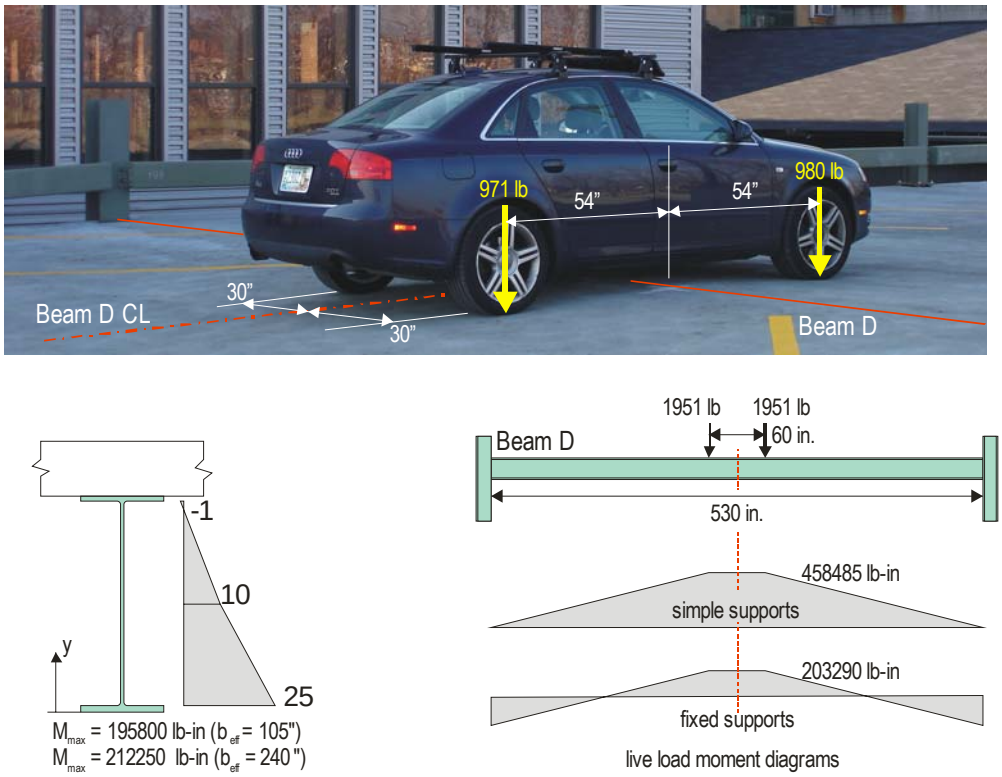

Figure 6.3 Live load test: December 30, 2006.

6.2.2. "Two Vehicle" Test – January 12, 2007

A second live load test was conducted on all beams January 12, 2007. In this test, An AUDI A4 having specified front and rear GAVW of 1960 lbs and 1942 lbs, respectively, and an Oldsmobile Alero having specified front and rear GAVW of 1714 lbs and 1402 lbs, respectively, were positioned over the center of each beam in turn as shown in Figure 6.4. The strains resulting only from the application of the live load are given in Table 6.1. From the live load strain distribution obtained, the location of the beam neutral axis was determined and the resulting applied moment found in the same manner as indicated in Section 6.2.1. The live load moment resulting from each loading case is shown in Table 6.1. Based on the observed strain behavior and neutral axis locations, all beams are clearly behaving as composite members having ends largely restrained from rotation. This observation is discussed in Section 7.4.

Table 6.1 Results of live load test: January 12, 2007.

	Beam at midspan (gage 9)		
	B	**C**	**D**
observed tension flange strain (microstrain)	173[1]	42	44
apparent neutral axis location, y (inches)	22.2	22.9	26.9
apparent moment (assume b_{eff} = 105") (lb-in)	[1]	324,000	289,000
apparent moment (assume b_{eff} = 240") (lb-in)	[1]	351,800	313,700
applied moment (simply supported) (lb-in)	815,500		
applied moment (fixed supports) (lb-in)	335,200		

[1] Beam B strain is believed to be an incorrect reading

6.3 Gage Integrity

As discussed in Section 4 and shown in Figure 4.3, field conditions resulted in damage to some of the strain gages. The following gages where excluded from the data analysis due to inconsistent and erroneous readings indicating damage: B4, B7, B13, C5, D5, D6, D10 and D14. Additionally gages B1 and C9 returned multiple inconsistent readings although they later appeared to be operational. Other gages were observed to return single erroneous readings; these are attributed to the data acquisition process and the likelihood that one of the screw terminals was inadequately tightened. Inconsistent data has been discarded in every case.

As indicated in Table 5.1, an effort was made to minimize the variance in temperature during data acquisition, thereby minimizing the temperature correction necessary[2]. Additionally, data was typically acquired in the afternoon when the ambient temperature had stabilized. Nonetheless, some variability in the data associated with temperature is evident despite the temperature correction made. This is most notable on the days where the extreme temperatures were observed: November 27 and December 8 when the recorded ambient temperatures were 67°F and 28°F, respectively.

[2] Indeed, milestone J was delayed until the temperature was in the vicinity of 45°F. The ambient temperature for the preceding week was below freezing as shown in Figure 5.1.

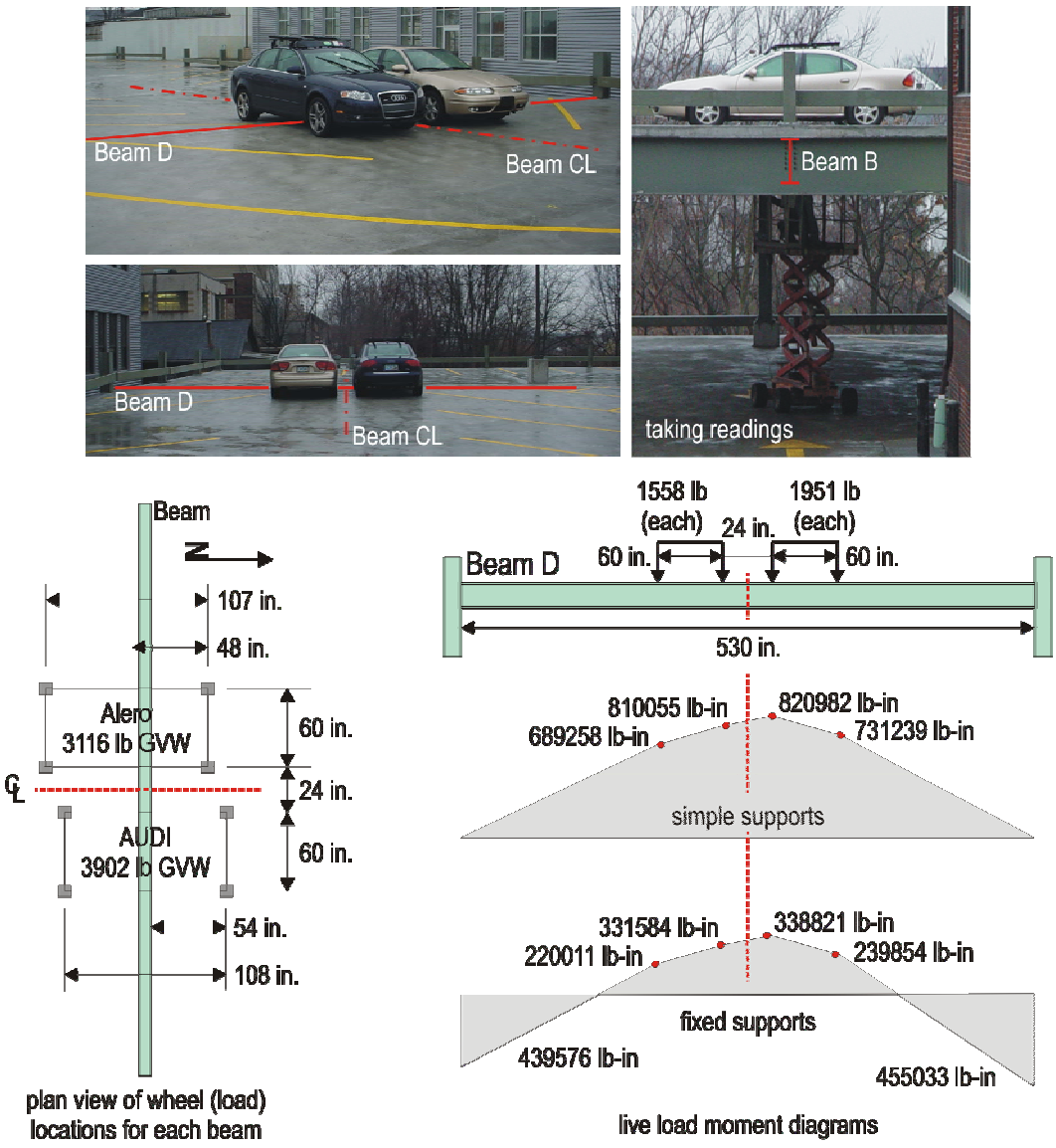

Figure 6.4 Live load test: January 12, 2007.

7. Discussion of Test Results

7.1 Effective Width of Slab

For a steel beam having a composite concrete deck (flange), it is necessary to determine the effective width of the flange contributing to the composite beam behavior. This value is termed b_{eff} and is the total width of composite slab centered over the beam. For the post-tensioned structure considered, different values of b_{eff} are appropriate for use at different stages of the construction process.

7.1.1 Effective width while formwork is in place ($b_{eff, form}$)

Between the time that the concrete deck hardens and begins acting compositely with the underlying beams and the time at which the formwork is removed, a limited portion of the deck slab is able to act in a composite manner with the beam. The formwork supports the majority of the slab and is stiffer in resisting gravity loads than the beam, therefore only that portion of the slab tributary to the beam will affect the load carrying capacity of the beam. In this work, this effective width, $b_{eff, form}$ is taken as equal to 36" based on the observed spacing of the formwork as shown in Figure 7.1.

Figure 7.1 Location of form shores at Beam B
(photo taken as shores are being removed and coincides with the photo shown in Figure 5.4).

7.1.2 Code prescribed effective width

Once there is no supplemental support from the formwork or shores, the beams behave in a composite manner. Table 7.1 gives the code-prescribed values of effective width for both the current AISC and ACI standards. The values given are for Beams B, C and D having a 6" deep slab.

Table 7.1 Effective width calculations.

requirement	AISC 2005 *Specification for Structural Steel Buildings* I3.1a	ACI 318-05 *Building Code Requirements for Structural Concrete 8.10.2*
1/4 beam span	0.25(45'-2") = 135"	
beam spacing	240"	n.a.
clear distance to next web	n.a.	240"
16 times slab thickness plus beam width	n.a.	16(6) + 9 = 105"

For design the value for b_{eff} would be taken as 135" (AISC) or 105" (ACI). However design is based on an ultimate load case in which case some level of slab degradation and cracking is expected. For the dead load and relatively low service load cases considered in this work, the effective width is more appropriately taken as the area tributary to each beam, that is b_{eff} = 240".

7.2 Composite Section Properties

Table 7.2 provides a summary of composite section properties calculated using different parameters for beams C and D (W24x76 steel section).

Table 7.2 Composite section properties.

f_c'	$n = E_s/E_c$	b_{eff}	I	y	S_t	S_b	S_t*	S_b*
psi		in	in^4	in	in^3	in^3	in^3	in^3
bare steel			2100	12.0[1]	-176	176	-187	187
3000	9.3	36	4651	10.3	-1073	238	-1272	246
4000	8.0	36	4669	9.6	-1299	241	-1602	249
4000	8.0	240	6294	4.6	4536	258	3044	265
5000	7.2	36	4969	9.4	-1466	242	-1834	251
5000	7.2	105	6092	6.0	∞	255	9600	263
5000	7.2	135	6282	5.5	12105	257	5240	265
5000	7.2	240	6614	4.5	4424	260	3041	268

y = depth of neutral axis measured from top of concrete (i.e. top of steel = y = 6.0")
S_t = elastic section modulus measured to top of steel
S_b = elastic section modulus measured to bottom of steel
S_t* = elastic section modulus measured to *bottom of top flange* (gage location)
S_b*= elastic section modulus measured to *top of bottom flange* (gage location)
[1] no concrete, therefore y is at midheight of W24 section

7.3 Predicted Behavior

Based on the composite section properties presented in Table 7.2, the expected stress and strain behavior of Beams C and D at midspan are presented in Table 7.3. The length of Beams C and D is taken as 44'-2". Table 7.3 is based on *simply supported end conditions* and thus represent upper bound values. To obtain values for fixed-fixed end conditions for the beam midspan, the tabulated values of midspan moment may be factored by 0.33; representing a lower-bound value. In all cases the stresses are determined at the gage locations (i.e.: using values of S_t* and S_b* from Table 7.2) and E = 29000 ksi.

Table 7.3 Predicted steel stress and strain behavior.

Load Case	Behavior	Moment	top flange		bottom flange	
			stress	strain	stress	strain
		lb-in	psi	με	psi	με
steel self weight	noncomposite	223257	-1194	-41	1194	41
concrete with shores in place	noncomposite	881616	-4715	-163	4715	163
full concrete load	noncomposite	4612319	-24665	-851	24655	851
full concrete load, b_{eff} = 105"	100% composite	4612319	480	17	17537	605
full concrete load, b_{eff} = 135"	100% composite	4612319	880	30	17405	600
full concrete load, b_{eff} = 240"	100% composite	4612319	1517	52	17210	593

stress = moment/S*
strain = stress/29

7.4 Predicted versus Observed Behavior

Table 7.4 provides a comparison of predicted bottom flange strain values (tabulated in Table 7.3) and observed values shown in Figure 6.1(c) for Beam D. The bottom flange at midspan is chosen for comparison because a) simple and fixed end moments may be directly compared and the degree of fixity established; and b) tension flange strains are greater and thus error and noise are proportionally reduced. In the cases shown in Table 7.4, the effect of steel dead load is assumed to result in a 41 microstrain strain. Since data is zeroed, based on this value, it is necessary to add this value to the observed strains; this has been done in Table 7.4.

Table 7.4 Comparison of observed and predicted behavior at midspan of Beam D.

Milestone	Load Case	**Strain at top of bottom flange at midspan** (gage 9)		**Observed** / Predicted
		Predicted	**Observed**	
Dead Load Tests				
B	concrete with shores in place	163	163	1.00
F	full concrete load	593 (b_{eff} = 240")	641	1.08
H			512	0.86
I			573	0.97
J			553	0.93
Live Load Tests (only live load strains are shown)				
I*	AUDI test	59 (simple supports)	25	0.42
		26 (fixed supports)		0.96
J*	Two vehicle test	105 (simple supports)	44	0.42
		43 (fixed supports)		1.02

The results presented in Table 7.4 illustrate the following aspects of the beam behavior:

1. the assumption of approximately 36" of fresh concrete being carried by the beam is reasonable (Milestone B)
2. dead load is carried primarily in simple bending (Milestones F-J)
3. the beam behaves as a fixed ended beam in resisting the relatively small live loads used (Milestones I* and J*)

The apparent discrepancy between observation 1 and 2 (above) results from the fact that the top and bottom flange angles used where beams frame into columns were not actually tightened at the time of placing the concrete or later removing the forms. It is not clear when and/or if these angles were tightened, however the presence of the composite slab and the low live loads used should be expected to result in a beam "made continuous for live load" regardless of the presence of these angles. The observed behavior supports this observation.

A final comment on Table 7.4 is warranted. The post-tensioning force is introduced at Milestone C and thus should affect all subsequent milestones. However, as will be shown in the following section, the resulting compression strains from the PT forces are largely "decompressed" (undone) by the PT-induced flexure introduced at Milestone F. As will be shown, this is partially an artifact of the force levels and geometry of the structure considered.

7.5 Post-tension-induced stresses

The following discussion is presented in the order in which the post-tensioning operation is carried out and assumes the general scenario whereby the concrete is placed, the PT is pulled and then the forms are released. Calculations are provided using Beam D as an example.

7.5.1 Post-tensioning operation

During the initial post-tensioning operation the slab remains shored. Axial stresses in the deck system are self-equilibrated resulting in internal stresses associated with the axial force (i.e., the P_i/A component). Flexure-induced stresses associated with the eccentricity of the PT tendons (i.e., the P_ie/S component), however, are largely resisted by the stiff formwork system (recall that the formwork is considerably stiffer than the beam in resisting vertically oriented forces). Thus only the axial stresses are carried in the beam at the time of post-tensioning. Based on these

assumptions, the expected axial strain in the beam and slab due to post-tensioning is 47 microstrain (see calculations below). As reported in Figure 6.2, the observed axial strain is on the order of 40 microstrain. Factors affecting both the predicted and observed values include a) the expected variability in concrete properties at an early age; and, the assumption of 100% composite behavior being developed in carrying axial load. Generally, one would expect the measured steel strains to be lower than the concrete strains. In this light, and based on previous experience, the observations and predictions correlate remarkably well.

Calculations – Axial strain due to initial post-tensioning (forms in place)

initial PT force in single strand	$f_{pi} = 0.73 f_{pu} = 30{,}200$ lbs	…see Section 6.1
tendons tributary to Beam B	8 tendons	
total PT force tributary to Beam B	$P_i = 8 \times 30{,}200 = 241{,}600$ lbs (compression)	

gross transformed area of 240" slab width and Beam B

area of concrete	$A_c = 240 \times 6 = 1440$ in^2	
modular ratio at time of PT pull	$n = E_s/E_c = 29 \times 10^6/(3.1 \times 10^6) = 9.3$	
E_c at time of PT pull	$E_c = 57000(3000)^{1/2} = 3.1 \times 10^6$	…assume $f_c = 3000$ psi
transformed area of steel	$A_{s\,tr} = nA_s = 9.3 \times 22.4 = 208$ in^2	…W24x76
gross transformed area	$A_{g\,tr} = A_c + A_{s\,tr} = 1440 + 208 = 1648$ in^2	

axial strain due to initial post-tensioning

$\varepsilon_{PT\,axial} = P_i/A_{g\,tr}E_c = 241{,}600/(1648 \times 3.1 \times 10^6) = 47$ microstrain (compression)

7.5.1.1 Rigorous analysis of post-tensioning operation

The assumption promulgated above that the PT operation results in only axial stresses provided the slab remains shored is, admittedly, an idealization. A rigorous analysis of the problem may be made by considering the shored system as a beam on elastic foundations subject to an axial force moments at each end. The elastic foundation, representing the shores, is assigned a stiffness in terms of a unit stress to cause a unit deflection (psi/in, for instance). This stiffness is effectively the axial stiffness of the shoring system as indicated in Figure 7.2. In general, this stiffness will be relatively large since it effects the vertical deflection of the forms when placing the concrete deck. An example of estimating the effective stiffness of the shoring system is provided below:

Calculations – Equivalent elastic foundation stiffness of slab shore system

Assume slab shores are provided by 15 foot tall scaffold-type shores having 2 ½" STD pipe legs (A = 1.59 in^2). The scaffold foot print is 96" x 24" and the units are spaced at 24" in both directions. The resulting tributary area to a single scaffold leg is therefore: 60" x 24" = 1440 in^2.

Load to cause axial deflection $\Delta = 1$": $P = \Delta AE/L = (1)(1.59)(29 \times 10^6)/(15 \times 12) = 256{,}000$ lbs

Elastic foundation stiffness: $k_0 = 256{,}000/1440 = 178$ psi/in

The shore stiffness has no effect on the axial component of the PT force; thus the axial stress in the system may be calculated as in Section 7.5.1. The effect of the induced moment is determined based on the behavior of a beam on elastic foundations. A standard solution to the problem shown in Figure 7.2(c) is provided in *Roark's Formula's for Stress and Strain* (Young and Budynas 2002) as shown below. It is clear from these calculations that stresses due to the PT induced moment are negligible provided the shores remain engaged.

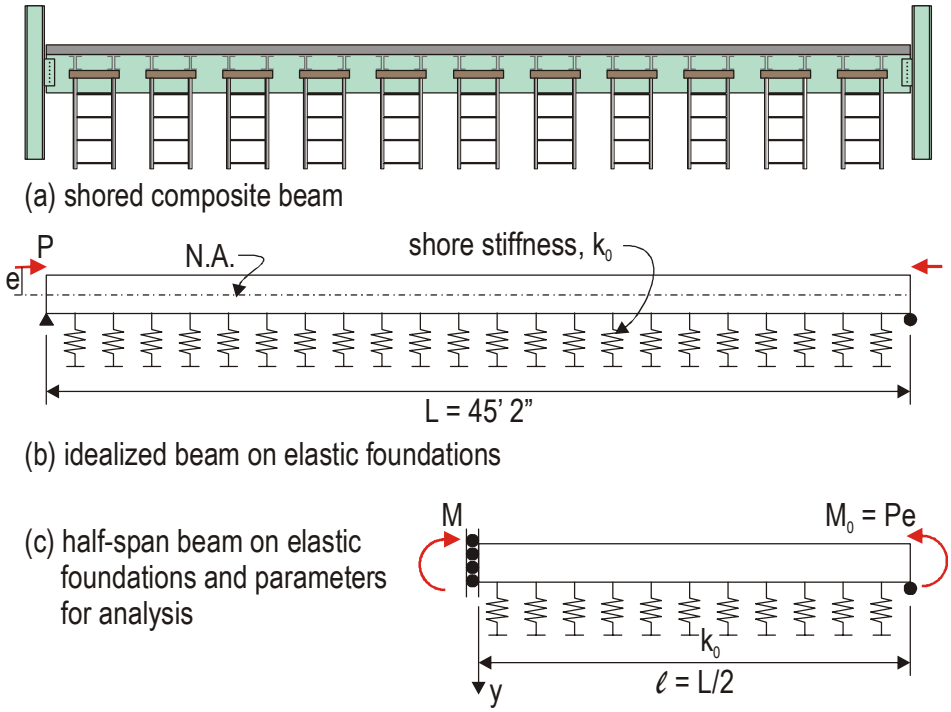

Figure 7.2 Modeling shored beam as beam on elastic foundations.

Calculations – Midspan moment for beam on elastic foundations
Considering the entire width of slab tributary to a beam (from Table 7.2, using f_c' = 4000 psi):

b_o = 240 in. I = 6294 in^4 E = 29,000,000 psi ℓ = (45' 2")/2 = 271 in.

$$\beta = \left(\frac{b_o k_0}{4EI}\right)^{1/4} = \left(\frac{240x178}{4x29x10^6 x6294}\right)^{1/4} = 0.0156 \quad \text{and } \beta\ell = 4.215 \qquad \textit{Roark's}$$

Midspan moment: $$M = M_0 \frac{-\cosh\beta\ell\cos\beta\ell}{1+\sinh^2\beta\ell-\sin^2\beta\ell} = -0.0141 M_0 \qquad \textit{Roark's}$$

Midspan vertical deflection: $$y = \frac{M_0}{2EI\beta^2}\frac{-\sinh\beta\ell\sin\beta\ell}{1+\sinh^2\beta\ell-\sin^2\beta\ell} = 2.8x10^{-10} M_0 \qquad \textit{Roark's}$$

M_0 = Pe = (8 x 30200) x 1.6 = 386,560 lb-in

Thus the midspan moment, M = -5454 lb-in, resulting in an extreme tension flange stress of 21 psi and corresponding strain of less than 1 με.

Clearly a variety of assumptions can be made in this calculation; the effective stiffness of the beam, I, the actual applied moment, M_0, and the vertical stiffness of the shores, k_0, being the most significant. For any reasonable case, however, the extreme tension flange stress did not exceed 10% of the stress due to the axial component of the PT force.

7.5.2 Release of formwork

Upon the release of the formwork, the flexure-induced stresses resulting from the eccentric application of the PT are transferred from the formwork shores to the beam. At this stage, the concrete has aged further resulting in a higher strength and stiffness which pushes the composite neutral axis upwards as the concrete continues to age. This effect can be seen in Table 7.2 as the concrete strength increases from 3000 to 5000 psi. If it assumed that the effective width of the slab is 240" and the concrete strength has attained a strength of 4000 psi at formwork release the additional strains transferred to the top and bottom flange of the beam (at the gage locations) are 4 and 50 microstrain, respectively.

For the beam and slab geometry considered, the flexure-induced strains associated with post-tensioning are approximately 10% of those associated with the transfer of full dead load to the beams (as the forms are released) as shown in Table 7.3. Additionally, for the geometry considered, the bottom flange strain associated with axial PT force (P_i) and that associated with flexure-induced forces (P_ie/S_b) virtually cancel each other. The top flange axial-induced strains are reduced marginally since the neutral axis (in this case) has migrated into the slab.

Calculations – Flexure-induced strain due to post-tensioning (at release of forms)

total PT force tributary to Beam B $P_i = 8 \times 30{,}200 = 241{,}600$ lbs (compression) … see above

assuming the tendon is at the mid-depth of the slab (y = 3), the eccentricity of PT force, e = 1.6"

induced moment $P_ie = 386{,}560$ lb-in

resulting flexure-induced strain in top flange

$\varepsilon_{PT,\ flex\ top} = (P_ie/S_t^*)/E_s = (386{,}560/3044)/29 \times 10^6 = 4$ microstrain (tension)

resulting flexure-induced strain in bottom flange

$\varepsilon_{PT,\ flex\ top} = (P_ie/S_t^*)/E_s = (386{,}560/265)/29 \times 10^6 = 50$ microstrain (tension)

7.6 Summary of Procedure for Assessing PT-induced Stresses

7.6.1 PT pulled while slab shored

If the PT is pulled while the slab remains shored (Figure 7.3(a), left), only the axial PT force is transferred to the steel beam. In this case the induced strain may be calculated as:

$$\varepsilon_{PT\ axial} = P_i/A_{g\ tr}E_c \qquad \text{Eq 7.1}$$

where P_i is the PT force tributary to the beam considered
$A_{g\ tr}$ is the gross transformed area of the tributary slab and steel beam composite section
E_c is the concrete modulus at the time of PT pulling.

Once the shores are released (Figure 7.3(a), right), the flexure-induced strains are transferred to the beam:

$$\varepsilon_{PT,\ flex} = (P_ie/S)/E_s \qquad \text{Eq 7.2}$$

where e is the eccentricity from the tendon centroid to the composite neutral axis
S is the appropriate section modulus for the location of interest in the section

It is noted that values of E_c will increase and the location of the neutral axis will migrate upwards as the structure ages resulting in a different basis for Equations 7.1 and 7.2.

7.6.2 PT pulled while slab is unshored

In this case the actions of Equation 7.1 and 7.2 occur simultaneously (Figure 7.3(b)) and all material properties are evaluated at the time of PT pulling:

$$\varepsilon_{PT,} = P_i/A_{g\,tr}E_c + (P_i e/S)/E_s \qquad \text{Eq 7.3}$$

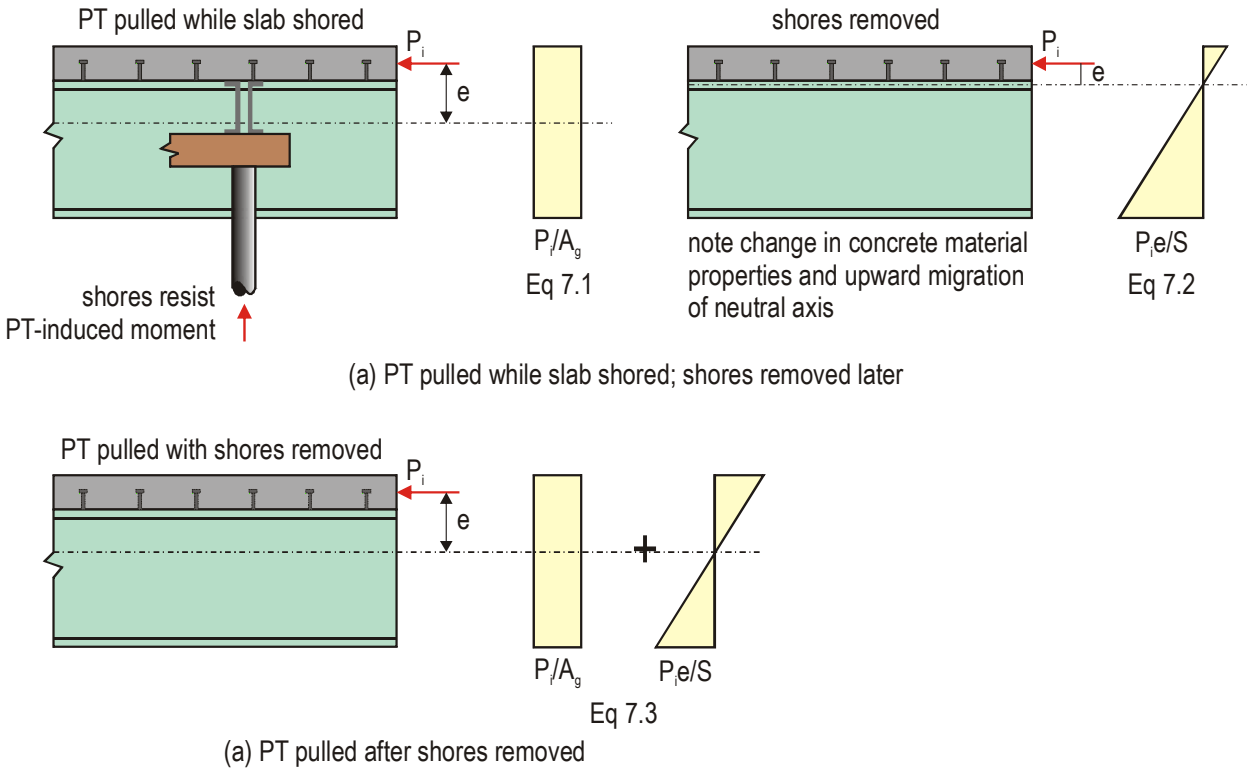

Figure 7.3 PT-induced stresses.

7.6.3 Non-composite slab

In the case were no shear transfer between the slab and supporting beam is provided, the PT forces will only induce stresses in the slab as shown in Figure 7.4(a).

7.6.4 *AISC Design Guide 18* Figure 3.12 misconception

The existing Figure 3.12 in *Design Guide 18* (reproduced in Figure 7.4(b)) shows the PT-induced flexural stresses carried by the steel beam in a non-composite manner. As indicated in *AISC Design Guide 18*, **this force resisting mechanism is not possible.**

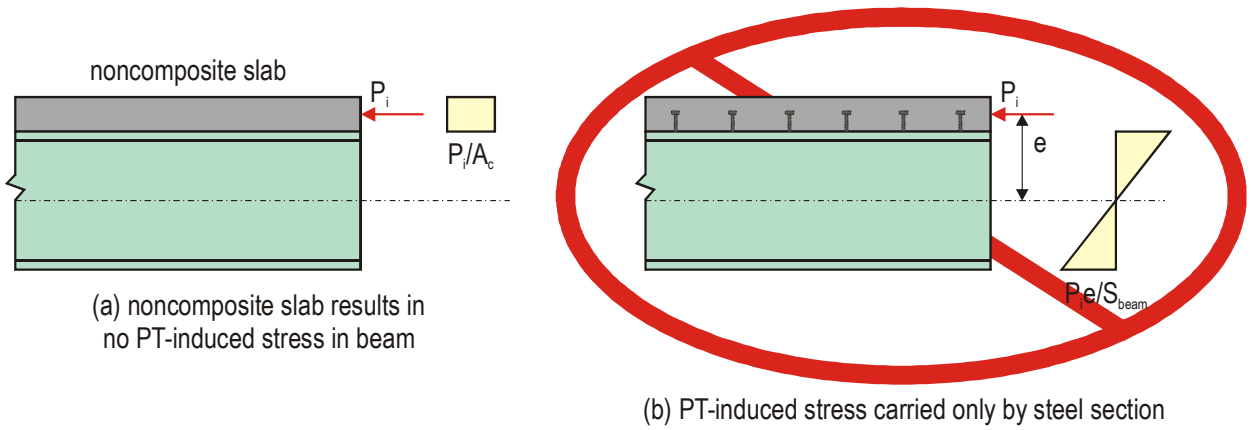

Figure 7.4 Noncomposite and incorrect PT-induced stress distribution.

8. Summary and Conclusions

This report summarizes a program of monitoring the during- and post-construction behavior of a steel-framed open parking deck having a cast-in-place post-tensioned concrete slab. Monitoring was carried out over two months beginning following steel erection and ending approximately three weeks following completion of the structure. Data was acquired at a variety of stages through the construction process. Additionally, two live load tests were conducted. The objective of this field study was to quantitatively assess the effect that slab post-tensioning forces have on their supporting steel members. The following conclusions were drawn with respect to the objective of this work in relation to existing AISC-promulgated design guidance:

1. As shown in Section 7, observed behavior agreed well with behavior predicted using the intent of the current AISC-recommended design process.
2. The AISC recommendations, forming Section 3.3.2.1 of *Design Guide 18* are appropriate in their present form although may not be universally conservative as written. Nonetheless, the levels of stress considered are sufficiently low that they should have little significant effect on design or behavior of the structural system.
3. For the beam and slab geometry considered, the flexure-induced strains associated with post-tensioning are approximately 10% of those associated with the transfer of full dead load to the beams (as the forms are released). Additionally, for the geometry considered, the bottom flange strain associated with axial PT force and that associated with flexure-induced forces virtual cancel each other. The top flange axial-induced strains are reduced marginally since the neutral axis (in this case) has migrated into the slab.

General conclusions drawn form this work are drawn:

4. Post-tensioned concrete slabs are known to be more durable than non-tensioned slabs. In a steel-framed parking deck, the post-tensioning is provided to affect this durability and not to provide any enhanced structural load-bearing capacity.
5. While the form shores are in place, the steel beams carry only concrete deck loads tributary to the beam *relative to the shores*.
6. Dead loads are resisted in simple bending – resulting stresses may be obtained assuming simple end supports.
7. Relative low service live loads are resisted in a manner approaching fixed-ended flexure; stresses may be obtained accordingly. This behavior is analogous to a bridge being made “continuous for live load”.
8. If shores are in place during the post-tensioning operation, only axial stresses are effectively transferred to the supporting steel beams. These stresses may be calculated based on an equivalent transformed gross section analysis.
9. The shores are sufficiently stiff to resist flexural stresses induced by the post-tensioning operation.
10. Once the forms are released, post-tension-induced flexural stresses are transferred to the supporting steel beam. These stresses should be assessed using a transformed sections analysis and material properties at the time of the form shore release.
11. Typically accepted methods for calculating post-tensioning losses appear to be appropriate for assessing post-tension-induced stresses.

9. Cited References

Aalami, B.O. (2004) Prestressing Losses and Elongation Calculations, *ADAPT, T9-04*, September 2004 (revised October 2004), 16 pp.

American Concrete Institute (ACI) (2005) *ACI 318-05 Building Code Requirements for Structural Concrete*, ACI, Farmington Hills, MI.

American Concrete Institute (ACI) (1998) *ACI 308.1-98 Standard Specification for Curing Concrete*, ACI, Farmington Hills, MI.

American Institute of Steel Construction (AISC) (2005) *Steel Construction Manual* 13th edition. AISC, Chicago, IL.

ASTM International (2004) *C232-04 Standard Test Methods for Bleeding of Concrete*, ASTM International, West Conshohocken, PA.

ASTM International (2006) *C403-06 Standard Test Method for Time of Setting of Concrete Mixtures by Penetration Resistance*, ASTM International, West Conshohocken, PA.

Bakota, J.F. (1988) Parking Structure with a Post-tensioned Deck. *Engineering Journal* (American Institute of Steel Construction), Third Quarter 1988, pp 119-125.

Churches C.H., Troup, E.W.J. and Angeloff, C. (2003) Steel Framed Open-Deck Parking Structures, *Steel Design Guide 18*, American Institute of Steel Construction (AISC), 113 pp.

Englot, J.M and Davidson, R.I., (2001) Steel Framed Parking Garages Take Off at JFK and Newark International Airports, *Modern Steel Construction*, Vol. 44, No. 4, April 2001, 6 pp.

MacGregor, J.G. and Wight, J.K., (2006) *Reinforced Concrete: Mechanics and Design*, 4th edition, Pearson Scientific.

[A] New Structural System for Parking Decks (1974) *Modern Steel Construction*, Vol. 14, No. 2.

Poole T.S. (2004) *Curing of Portland Cement Concrete Pavements, Volume II Final Report*. FHWA-HRT-05-038.

Poole T.S. (2005) *Guide for Curing of Portland Cement Concrete Pavements*. FHWA-RD-02-099.

Simon, A.H. (2001) Unique Steel Framed Solution to Parking, *Modern Steel Construction*, Vol. 44, No. 4, April 2001, 3 pp.

Sontag, H. (1970) Steel Multi-Storey Garages, *Acier-Stahl-Steel*, Vol. 35, No. 11, pp 480-490.

Troup, E. and Cross, J. (2003) *Innovative Solutions in Steel: Open-Deck Parking Structures*, American Institute of Steel Construction (AISC), 29 pp.

Young, C.S. and Budnyas, R.G. (2002) *Roark's Formulas for Stress and Strain*, 7th edition, McGraw Hill.

Appendix A – Observed Strain Data

In the following Table, the observed strains, zeroed by the strain reported at Milestone A and corrected for ambient temperature are reported. Crossed-out entries indicate erroneous data as described in Section 6.3.

Milestone	Gage Number															
	ΔT	1	2	3	4	5	6	7	8	9	10	11	12	13	14	15
	BEAM B															
zero	0	1261	605	1205	~~171~~	460	1198	~~554~~	301	1657	1601	1572	849	~~1242~~	619	1142
A	0	0	0	0	~~0~~	0	0	~~0~~	0	0	0	0	0	~~0~~	0	0
B	60	98	74	60	~~40~~	43	80	~~44~~	99	75	164	42	115	~~87~~	80	74
C	144	73	102	79	~~23~~	17	19	~~-163~~	82	32	147	23	105	~~157~~	36	86
D	174	63	98	174	~~63~~	14	112	~~80~~	133	212	191	90	78	~~-54~~	~~-168~~	130
E	-54	~~-425~~	-118	-120	~~-147~~	-178	-159	~~-282~~	-117	~~-63~~	-135	-234	-129	~~-420~~	-190	-96
F	102	-47	63	16	~~-429~~	-4	~~-1019~~	~~-597~~	154	~~-100~~	55	97	-90	~~-24~~	-32	115
G	48	12	105	-60	~~167~~	62	365	~~-236~~	234	504	~~-446~~	216	397	~~447~~	24	154
H	48	14	90	145	~~-47~~	160	355	~~28~~	273	552	48	187	404	~~138~~	71	148
I	84	11	112	187	~~-30~~	191	364	~~-10~~	335	602	60	466	499	~~684~~	119	165
J	66	~~-348~~	105	185	~~-10~~	~~-162~~	347	~~-95~~	332	497	15	120	446	~~1286~~	75	154
J*	66	~~-347~~	109	194	~~-69~~	177	414	~~-98~~	366	670	16	142	469	~~1179~~	74	145
	BEAM C															
zero	0	1461	1142	1629	~~1081~~	705	1241	963	828	1529						
A	0	0	0	0	~~0~~	0	0	0	0	0						
B	60	42	81	77	~~70~~	51	86	47	-244	82						
C	144	9	148	82	~~79~~	-9	69	-6	9	58						
D	174	-39	125	186	~~134~~	25	101	-2	74	95						
E	-54	-454	-127	-91	~~-122~~	-287	-104	-165	-152	-105						
F	102	-3	124	239	~~56~~	188	446	-176	214	430						
G	48	~~-843~~	60	186	~~1~~	144	209	-174	192	406						
H	48	-370	66	192	~~6~~	99	480	-34	222	480						
I	84	3	108	230	~~130~~	-607	515	-123	251	551						
J	66	-42	73	216	~~-16~~	-296	506	-69	249	~~1198~~						
J*	66	-47	81	222	~~90~~	-20	553	-67	267	~~1240~~						
	BEAM D															
zero	0	845	1430	1609	36	~~1164~~	~~416~~	551	1239	882	~~1473~~	1168	1149	1279	~~165~~	956
A	0	0	0	0	0	~~0~~	~~0~~	0	0	0	~~0~~	0	0	0	~~0~~	0
B	60	71	87	187	119	~~84~~	~~95~~	47	39	163	~~47~~	-40	200	56	~~-130~~	110
C	144	45	123	124	129	~~-101~~	~~25~~	83	43	58	~~-496~~	44	101	97	~~-249~~	175
D	174	~~-307~~	79	213	63	~~108~~	~~276~~	60	93	178	~~-16~~	61	165	108	~~-540~~	175
E	-54	-292	-214	-95	-203	~~-695~~	~~-135~~	-158	-216	~~-836~~	~~-227~~	-158	-92	-112	~~262~~	-110
F	102	-25	314	50	-249	~~-2932~~	~~227~~	-56	188	600	~~-469~~	177	324	59	~~342~~	240
G	48	-159	51	61	-184	~~134~~	~~411~~	-178	47	366	~~-770~~	~~602~~	370	-118	~~311~~	103
H	48	-20	79	177	-27	~~-718~~	~~607~~	-116	139	471	~~-92~~	136	353	-24	~~693~~	182
I	84	-15	130	262	3	~~-1512~~	~~450~~	-105	151	532	~~-82~~	121	461	-74	~~178~~	238
J	66	-39	79	233	3	~~-136~~	~~437~~	-133	41	512	~~-81~~	42	380	11	~~32~~	90
J*	66	-37	89	234	62	~~102~~	~~461~~	-125	59	556	~~-109~~	134	465	-1	~~533~~	202

zero = actual instrument reading Milestone A

ΔT = strain temperature correction

Actual instrument readings may be recovered as follows: reported strain + zero - ΔT

Appendix B – Concrete Shrinkage and Cracking of Slab

This Appendix has been added to the report in response to review comments (paraphrased below) not directly associated with the findings of this report but relevant to concrete slab on steel girder parking decks nonetheless.

B.1 Restraint of Concrete Shrinkage Causing Cracks

One of the key durability issues [for PT decks] is the restraint of concrete shrinkage by the composite top flange of the steel beam, eventually causing cracking of the slab. Even though the concrete is prestressed, does the concrete go into tension due to the combined restraint and shrinkage?

The deck in the present was not instrumented to assess the effects of shrinkage. Regardless, it is not believed that results would not have been representative due to the environment under which the slab was placed and cured (see Section 3.2). Critically, it is noted that no curing measures where taken with this slab.

Nonetheless, shrinkage is an issue to be considered. Under reasonable curing conditions, CEB provides a method for assessing expected shrinkage strain. If it is assumed that 100% of shrinkage is restrained by the studs, it is a simple matter to compare the expected shrinkage strains with the strains to cause cracking. The following calculations are paraphrased from MacGregor and Wight, *Reinforced Concrete*, 4th edition.

$$\varepsilon_{shrinkage} = \left[-1.2\left[160 + 8\left(9 - \frac{1.2f_c'}{1450} \right) x10^{-6} \right] \left[1.55\left(1 - \frac{RH}{100} \right)^3 \right] \left[\frac{(t - t_s)}{350\left(\frac{2A_c}{4u} \right)^2 + (t - t_s)} \right]^{0.5} \right] \quad \text{Eq B.1}$$

where f_c' = the specified 28 day concrete strength;
RH = ambient relative humidity;
t = age of concrete (days);
t_s = age of concrete at end of steam curing phase;
A_c = sectional area of concrete (taken as 12" width of slab in this case); and,
u = perimeter of A_c exposed to air (taken as 12" top of 12" width of slab).

$$\varepsilon_{cracking} = \alpha \left[f_c' \left(\frac{t}{4 + 0.85t} \right) \right]^{0.5} \quad \text{Eq B.2}$$

where $\alpha = 6.5$ for $t > 10$ days; and,
$\alpha = 6.5(t/10)$ for $t < 10$ days.

Figure B.1 shows the comparison of expected shrinkage strains and cracking strains estimated for the presently considered deck. It is clear that this slab is not expected to crack due to shrinkage. The 47 microstrain jump in strain at day 5 represents the application of the post tensioning force.

These calculations are exceptionally conservative in as far as the demonstrated composite nature of the deck indicates that 100% of the shrinkage is not restrained but rather a portion is free shrinkage. In general, it is not anticipated that restrained concrete shrinkage will result in cracks in the type of deck investigated in this report.

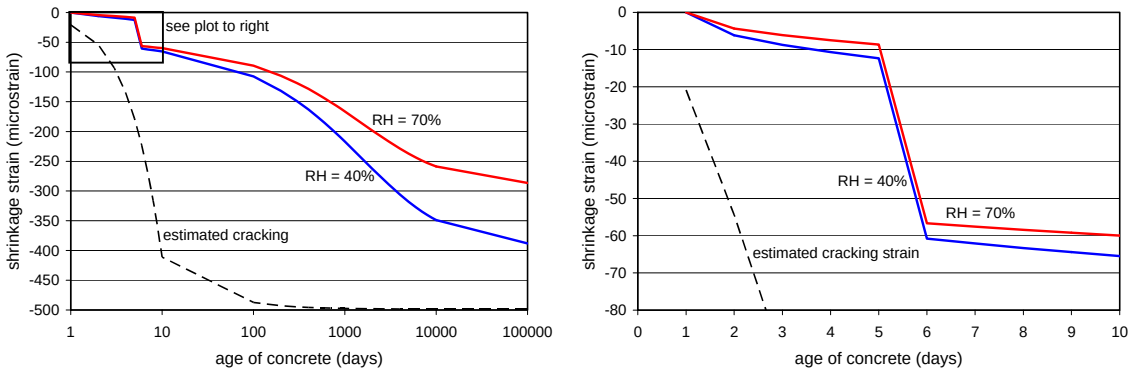

Figure B.1 Predicted shrinkage strains and estimated cracking strains.

B.2 Plastic Shrinkage Cracking

On a parking deck located in [a relatively dry climate], there were a number of shrinkage cracks on the roof deck (none on the floors below). It is [understood] that these cracks occurred shortly after the concrete was post-tensioned. [The cracks were attributed to] exposure to the sun and the very dry atmosphere in the area. These cracks indicate that there is a restraining effect to the concrete by the steel.

Plastic shrinkage cracks (PSC) appear on the surface of fresh concrete soon after it is placed. These cracks usually appear on horizontal surfaces and are characterized as parallel, relatively shallow, cracks about 12" to 36" apart which do not generally intersect with the slab perimeter. PSC usually results when high evaporation rates cause the concrete surface to dry out before the initial set.

To predict PSC, the anticipated evaporation rate is compared to the expected rate of bleed water coming to the concrete surface during the time of initial concrete set (TOS). If at any time during the TOS, the cumulative evaporation exceeds the cumulative production of bleed water, the surface becomes dry and PSC may occur. This is shown schematically in Figure B.2. PSC is more critical in high-performance concrete mixes where the inclusion of supplementary cementitious material (specifically silica fume) retards bleed water.

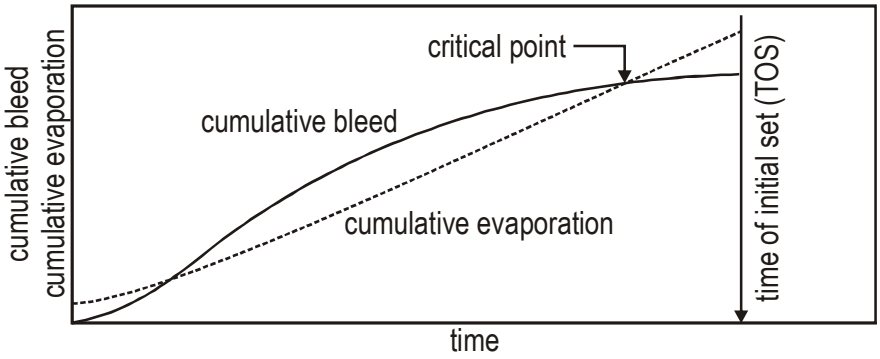

Figure B.2 Cumulative bleed and evaporation as function of time (after Poole 2006).

To mitigate PSC, misters, curing mats, chemical curing compounds or evaporation reducing admixtures may be used to mitigate the effects of evaporation. Another effective method of mitigating PCS is to reduce the concrete placement temperature.

The time of set, TOS, may be determined from ASTM C403 *Standard Test Method for Time of Setting of Concrete Mixtures by Penetration Resistance*. The rate of bleed water formation is determined by ASTM C232-04 *Standard*

Test Methods for Bleeding of Concrete, or may be estimated based on the water-cement ratio, w/c, of the mix and the thickness of the slab, t (Poole 2004):

bleed rate in units of $lb/ft^2/h = (0.027 \times w/c - 0.008)t$ Eq B.3

Finally, the evaporation rate may be found from a nomograph provided in ACI 308.1 *Standard Specification for Curing Concrete* (Figure B.3). As a rule of thumb, evaporation rates exceeding 0.06 $lb/ft^2/h$ require mitigating procedures (Poole 2006).

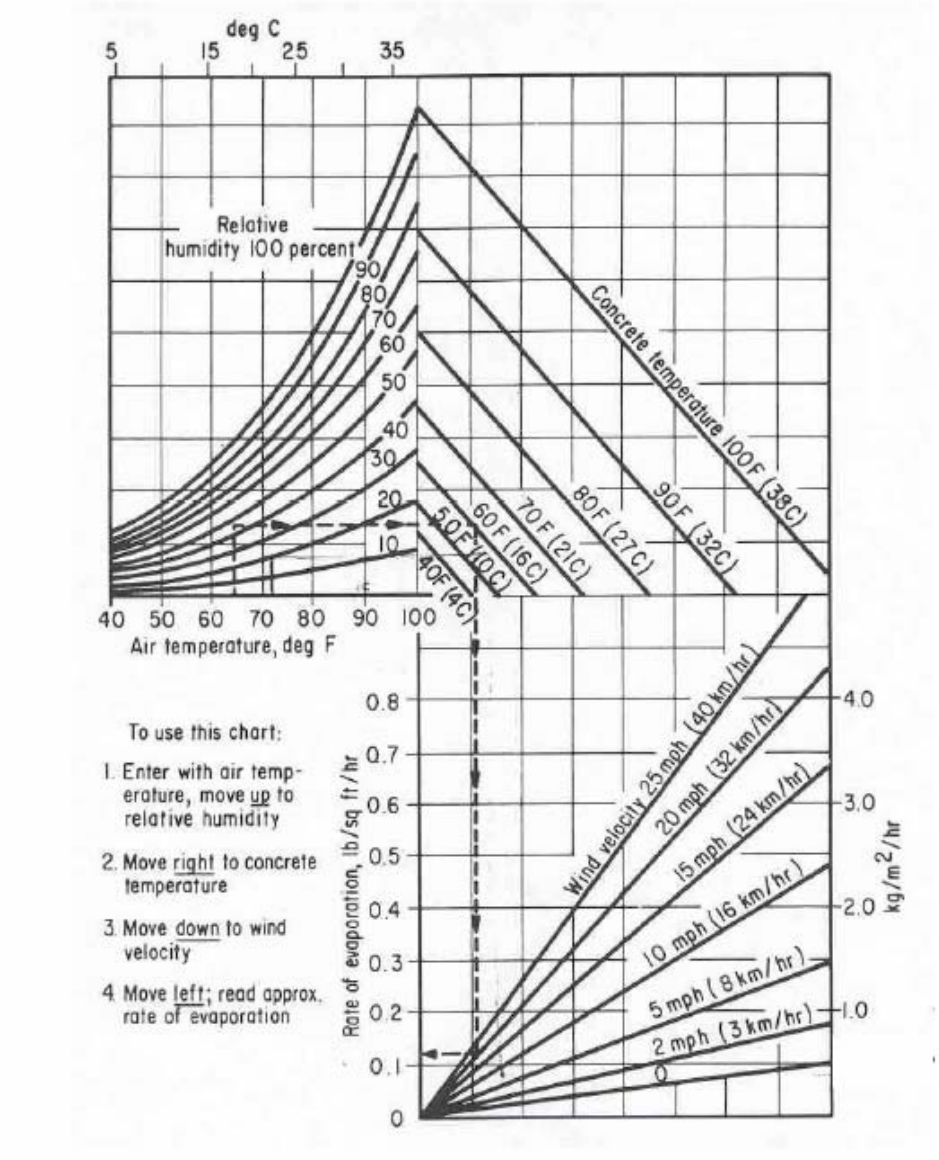

Figure B.3 Evaporation rate nomograph from ACI 308.1.